

AMERICAN UNIVERSITY OF BEIRUT

PROGNOSIS OF LAMB WAVE REFLECTIONS IN
COMPLEX GEOMETRY STRUCTURES

by
RAWAD ADEL MALAEB

A thesis proposal
submitted in partial fulfillment of the requirements
for the degree of Master of Engineering
to the Department of Mechanical Engineering
of the Maroun Semaan Faculty of Engineering and Architecture
at the American University of Beirut

Beirut, Lebanon
October, 2020

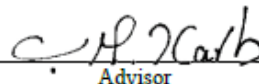
AMERICAN UNIVERSITY OF BEIRUT

PROGNOSIS OF LAMB WAVE REFLECTIONS IN
COMPLEX GEOMETRY STRUCTURES

by
RAWAD ADEL MALAEB

Approved by:

Dr. Mohammad Harb, Assistant Professor
Mechanical Engineering



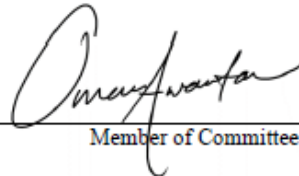
Advisor

Dr. Samir Mustapha, Associate Professor
Mechanical Engineering



Member of Committee

Dr. Omar Awartani, Assistant Professor
Mechanical Engineering



Member of Committee

Date of thesis defense: October 12, 2020

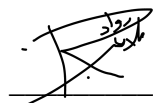
AMERICAN UNIVERSITY OF BEIRUT

THESIS RELEASE FORM

Student Name: Malaeb Rawad Adel .
Last First Middle

I authorize the American University of Beirut, to: (a) reproduce hard or electronic copies of my thesis; (b) include such copies in the archives and digital repositories of the University; and (c) make freely available such copies to third parties for research or educational purposes:

- As of the date of submission
- One year from the date of submission of my thesis.
- Two years from the date of submission of my thesis.
- Three years from the date of submission of my thesis.



October 15, 2020

Signature

Date

ACKNOWLEDGEMENTS

I would like to genuinely Thank Dr. Mohammad Harb for his guidance and encouragement through my master's degree. It was an honor to have him as my advisor and work with him. Thank you Dr. Harb for your support.

I also would like to thank my committee members Dr. Samir Mustapha and Dr. Omar Awartani for their advice and comments. Additionally, my fellow graduate students Elie Mahfoud, Jad El Najjar, Aussama Moudad, and Yasmine Baghdadi. Special thanks to my friends Waddah Malaeb, Dr. Eyad Faysal, Dr. Hadi Sareddeen, and Rayan Bou Mjahed for being always there to support and encourage me along the way.

I would also like to deeply thank my family for their support and help throughout my education.

ABSTRACT OF THE THESIS OF

Rawad Adel Malaeb

for

Master of Engineering

Major: Mechanical Engineering

Title: Prognosis of Lamb Wave Reflections in Complex Geometry Structures

Lamb waves are highly used in Structural Health Monitoring systems and are commonly studied to investigate the mechanical properties and integrity of different structures. The reflections from the boundaries of any studied structure complicate any data post-processing techniques and it is almost impossible to eliminate such reflections when working with small-sized structures. In addition, the more complex the geometry is the more reflections from edges and bents appear. This study focuses on understanding Lamb wave's boundary reflections and the effect of a bent on the signal. Tests are done on aluminum plates of different sizes and geometries, a step towards moving to composite materials and more complicated structures. In this work, the boundary reflections of Lamb waves propagating a thin metallic plate are investigated and a new theoretical Lamb wave boundary reflection (LBR) theorem is proposed that accurately predicts all boundary reflections and generates a full field signal based on a virtual actuating and sensing network. The LBR theorem locates virtual actuators that are used to transform the distance covered by the wave during the boundary reflection into a direct distance from the virtual actuator to the sensor. Using commercially available software to generate the incident wave between an actuator and a sensor, the proposed boundary reflection theorem is then used to predict the overall signal including reflections from all boundaries. The predicted signals are first validated using finite element analysis which also assists to visualize and analyze the actuation, propagation, and reflection of the waves in the plate. Additionally, an ultrasonic piezoceramic contact transducer and non-contact laser Doppler vibrometer are utilized experimentally to verify the validity of the proposed technique. The predicted signals at different excitation frequencies have shown a very good agreement between the theoretically predicted, computational, and experimental results.

TABLE OF CONTENTS

ACKNOWLEDGEMENTS	1
ABSTRACT	2
ILLUSTRATIONS.....	5
TABLES	8
CHAPTER I	
INTRODUCTION.....	9
CHAPTER II	
LITERATURE REVIEW	13
A. Structural Health Monitoring (SHM) System.....	13
B. Guided Waves	16
C. Damage Detection Methods.....	18
D. Signal Processing Techniques.....	19
CHAPTER III	
EXPERIMENTAL AND NUMERICAL METHODOLOGIES	21
A. Lamb waves	21
1. Fundamentals of Lamb Waves	22
2. Dispersion Curves in Aluminum 1050	23
A. Signal Used	24
B. Experimental Setup	25
1. Effect of a perpendicular bent on lamb waves in an aluminum plate	27
2. The study of boundary reflection and attenuation of lamb waves in an aluminum plate	28

3.	Effect of the angle of the bent on lamb wave in an aluminum plate .	29
C.	The Chosen Frequencies	30
D.	The Numerical Models.....	30
1.	Effect of a perpendicular bent on lamb waves in an aluminum plate	30
2.	The Mesh	31
3.	The study of boundary reflection and attenuation of lamb waves in an aluminum plate	33
CHAPTER IV		
LAMB WAVE MODES AND BOUNDARY REFLECTION DETECTION		36
CHAPTER V		
LAMB WAVE BOUNDARY REFLECTION THEOREM		41
Chapter VI		
RESULTS AND DISCUSSION		44
A.	Effect of perpendicular bent on lamb waves in an aluminum plate	44
B.	The Study of Boundary Reflection and Attenuation of Lamb Waves in an Aluminum Plate.....	52
1.	The built-up signal according to the theorem.....	52
C.	Effect of the angle of the bent on lamb wave in an aluminum plate.....	56
1.	Effect of bent on the wave propagation.....	56
Chapter VII		
CONCLUSION AND FUTURE WORK.....		62
References		64

ILLUSTRATIONS

Figure

1. Group velocity dispersion curves for 3mm thick aluminum 1050.	24
2. Amplitude tuning curves for 3mm thick aluminum 1.....	24
3. (a) Five-peaked Hann-windowed tone-burst signal at 100kHz center frequency, (b) its frequency spectrum	24
4. (a) Five-peaked Hann-windowed tone-burst signal at 200kHz center frequency, (b) its frequency spectrum	25
5. Experiment setup for the experiment of a perpendicular bent on lamb waves in an aluminum plate	26
6. Experiment setup for the study of boundary reflection and attenuation.....	26
7. Actual and modelled Aluminum 1050 plates	27
8. Aluminum specimens used and PZTs placement configuration.....	28
9. Aluminum 1050 plate S showing the location of the line scans and the bent	29
10. Aluminum specimen used with the variation of bent angle.....	30
11. Mesh plot and meshed regions of Plate 2 in COMSOL model	33
12. ABAQUS and COMSOL FEA meshed models for plate S.....	35
13. Experimental (PZT and LDV) and theoretical captured signals at (a) 100 kHz and (b) 200 kHz, with their respective envelopes in (c) and (d).....	36
14. LDV measurements at 120 mm from the actuators in plates L and S at 100 kHz excitation frequency.....	38
15. LDV measurements at 120 mm from the actuators in plates L and S at 200 kHz excitation frequency.....	39

16. Generated and reflected wavefield (out-of-plane velocity) in plate S at 200 kHz excitation frequency captured from ABAQUS and COMSOL finite element models...	40
17. Virtual actuators with the assumed wave propagation.	42
18. Lamb wave boundary reflection (LBR) theorem sketch.	43
19. The effect of additional PZT discs placed between actuator and sensor	44
20. Experimental vs COMSOL results for both frequencies of 100 and 200 kHz for plate 1	46
21. Experimental vs COMSOL results for both frequencies of 100 and 200 kHz for plate 2	47
22. Experimental vs COMSOL results for both frequencies of 100 and 200 kHz for plate 3	47
23. Sensed signal in Plate 1 divided into packets where every packet is specified based on the obtained wave field.	49
24. Out-of-plane velocity wavefield showing excited S0 and A0 modes.....	49
25. Measured signal and envelope tracing.....	50
26. Measured signal envelopes for each plate	51
27. Reflection and transmission wave field from the right side bent-edge in Plate 2	51
28. Four pathway reflections in plate 2.....	52
29. A0 Lamb wave mode attenuation curve was generated experimentally.	53
30. Experimental setup schematic for calculating Lamb wave boundary reflection (LBR) coefficient.	54
31. Lamb wave boundary reflection (LBR) theorem versus experimental results at 100 and 200 kHz excitation frequencies in region 2 of plate L (a,b) and region 3 of plate L (c,d).....	55

32. Lamb wave boundary reflection (LBR) theorem versus experimental results at 100 and 200 <i>kHz</i> excitation frequencies in plate S.....	56
33. The line scan 1 for the plate at 100 <i>kHz</i> (a) 0 <i>degree</i> (b) 30 <i>degree</i> (c) 60 <i>degree</i> (d) 90 <i>degree</i> (e) 120 <i>degree</i> and (f) 150 <i>degree</i>	57
34. Top view of the plate showing the reflection from the bent (a) the first reflection and (b) the second reflection	58
35. The line scan 2 for the plate at 100 <i>kHz</i> (a) 0 <i>degree</i> (b) 30 <i>degree</i> (c) 60 <i>degree</i> (d) 90 <i>degree</i> (e) 120 <i>degree</i> and (f) 150 <i>degree</i>	58
36. Top and bottom reflection for the second line of scan showing how the bent blocks the way of the wave	59
37. The line scan 1 for the plate at 200 <i>kHz</i> (a) 0 <i>degree</i> (b) 30 <i>degree</i> (c) 60 <i>degree</i> (d) 90 <i>degree</i> (e) 120 <i>degree</i> and (f) 150 <i>degree</i>	60
38. The line scan 2 for the plate at 200 <i>kHz</i> (a) 0 <i>degree</i> (b) 30 <i>degree</i> (c) 60 <i>degree</i> (d) 90 <i>degree</i> (e) 120 <i>degree</i> and (f) 150 <i>degree</i>	61

TABLES

Table

1. Maximum element size and number of elements	32
--	----

CHAPTER I

INTRODUCTION

Nondestructive testing (NDT) is a growing area and a developing research field. NDT includes different evaluations to study the material properties and components without causing any damage to the material, and it is used in different applications in industry, medicine, geology, and other fields[1]. Billions of dollars are spent each year on maintenance for equipment and facilities, for example, a quarter of the commercial aircraft operational cost is going to maintenance and repairs[2].

Structural health monitoring (SHM) is an extended NDT which focus on health evaluation of a structure, damage detection occurring in real-time using permanently installed sensors[2, 3]. SHM may reduce maintenance and repair costs by eliminating unnecessary and unscheduled maintenance for aged structures. Including SHM in the design stage for new structures reduces the life cycle cost which increases safety and reliability, and reduces maintenance costs[2].

SHM intensely uses Lamb waves in the scanning process. Lamb waves are elastic guided waves that propagate in thin structures for long distances and they are sensitive to any changes in the structural properties of the material [4, 5]. However, it is a challenging field of study due to the existence of an infinite number of propagating modes that are highly dispersive[4, 6]. Besides, the extensive boundary reflections that are usually present in a structure complicates any data analysis and characterization of damage reflections after having all reflections combined[7].

Different industries are now focusing on laminated composites since they have increased strength and stiffness to weight ratio, increased toughness, and increased chemical and corrosion compared to conventional metallic materials.[8] Aircraft,

automotive, and space machines industries are attracted to such materials due to their improved properties so different inspections process will be needed. Several methods had been conducted to detect, localize, and characterize damage in composite materials[9, 10]. However, different challenges are faced regarding material characterization, in situ structural health monitoring, the complexity of composites, and inspection with unknown material properties.[8]

The huge computational power and the ability to interpret and understand the wave's computational results that evolved over the past two decades allow the tremendous advances made in ultrasonic guided wave technology and the SHM systems[11]. Computational methods have been increasingly used in solving wave propagation and vibration problems[12]. The finite element method (FEM), if used with the appropriate element size and boundary conditions, can give accurate and computationally efficient solutions. A numerical model can be built which helps in solving different complicated geometries and improves the ability to understand guided Lamb waves [11]. Harb and Yuan [13, 14] verified the characterization of Lamb waves in isotropic aluminum plates experimentally, theoretically, and computationally using COMSOL Multiphysics. Lu et al [15] had studied the forward and backscattering of Lamb waves by cracks experimentally and numerically using ABAQUS. Also, Travaglini et al [6] used ABAQUS to study the feasibility of detecting a crack on the circumference of a through-thickness hole with high order Lamb waves at high frequency. Such computational methods are very helpful in solving complex problems and offering a visual representation for propagating waves which is very valuable in the analysis process.

Most studies focus on studying lamb waves, their reflection, and damage detection in plates[7, 16-18], however, few works are done on reflections from bent[9, 19]. The focus on plate structures makes it difficult to analyze structures with complex geometry because it includes more reflections from edges. Also, the wave propagation in a bent object includes more attenuation due to interaction with bents compared to a plate.

This work studies the behavior of the first order symmetric (S0) and anti-symmetric (A0) Lamb wave modes in flat, single-side bent, and two-side bent thin aluminum plates experimentally and Numerically using COMSOL Multiphysics[20]. The results from the COMSOL Structural Mechanics Module are compared against each other to determine the effect of each bent boundary on the propagating waves. They are also compared with their respective experimental counterpart to evaluate the accuracy of COMSOL in predicting reflected waves from boundaries or damages. The current study, modeled in 3-D, shows contours of the wave fields representing the wave velocity components for each plate to trace and demonstrate each wave packet. In addition, it will present a new approach for approximating wave propagating signals based on a proposed Lamb wave boundary reflection (LBR) theorem. This can be a step forward to help recognize the reflection of damage after building the signal obtained from the boundary reflections and eliminating it from the main signal. This study will first present the experimental setup used. Next, the numerical work modeled in ABAQUS and COMSOL software will be proposed. The fundamental symmetric and antisymmetric Lamb wave modes are determined using the dispersion curves and Waveform Revealer software. The boundary reflections from different plate edges and corners were then studied experimentally and numerically. Finally, the boundary

reflection theorem was introduced and implemented with the incident wave predicted signal based on virtual actuating transducers. The predicted overall signals in a thin aluminum plate have shown an excellent match when compared with experimentally as well as numerically obtained signals. Finally, the future work that should be done.

CHAPTER II

LITERATURE REVIEW

A. Structural Health Monitoring (SHM) System

SHM is used for constructed objects in static and dynamic environments and it has different applications in mechanical[21, 22], aerospace[23], naval[24, 25] and civil[26, 27]. All industries try to detect the damage at an early time so they need to perform SHM to prevent disasters. There are many challenges related to the SHM techniques which include the development of methods to optimally define the number and location of the sensors, the ability to distinguish between changes caused from damage and from changes caused by changing environment or test conditions, identification of features to detect small damage levels, developing statistical methods to differentiate features from undamaged and damaged structures [28].

There are two kinds of SHM; the active SHM which directly assesses the health of the structure by detecting any existing damage, and the passive SHM measures various operational parameters and deduce the health of the structure based on the obtained parameters[2, 29]. Any SHM system consists of hardware which is the sensors and the associated instruments and software which consist of damage modeling and damage detection algorithms[30]. The SHM is formed of two components the Diagnosis and the Prognosis. According to Srinivasan et al.[30] the diagnosis gives an overview of the state of the constituent materials of the different parts and the whole assembly at every moment of the structure life which determines damages such as cracks and its location. While the prognosis procedure uses the diagnosis part and gives

more details and involves a computational analysis of the severity of the crack in terms of fracture mechanics parameters in addition to its remaining life.

The SHM is divided into five levels according to Srinivasan et al.[30], the first level is confirming the presence of damage and it is achieved by monitoring some of the structure's properties over time mainly the natural frequency of the body which will change in case of the presence of damage due to the reduction of stiffness but any damage that won't affect the stiffness significantly will not be detected. The second level detects the location of the damage and its orientation, where a known input is applied to the material and output is measured which will have an additional wave reflected from the damage. However, it is not possible to identify the reflection from the damage easily due to the number of boundary reflections or noise polluting the signal that is why different analysis techniques are used at this level. The third level tackles the severity of the damage after being detected, the Stress Intensity Factor (SIF) or the Strain Energy Release Rate (SERR) of the crack are estimated and compared with the threshold values. The crack will start growing if the SIF or the SERR reaches the threshold value. SIF is a quantity difficult to be measured and it should be correlated with the voltage histories obtained by the sensor to obtain the crack severity. The fourth level deals with decreasing or stopping the crack from growth and repair the body. Finally, the fifth level works on estimating the life of the structure after taking into consideration the work done in the fourth level.

SHM is used in Isotropic material that has properties independent of direction to detect damage, fatigue, and fracture. Eivani et al.[31] studied the severe plastic deformation processing using the twist extrusion on the high cycle fatigue and fracture mode of aluminum. LU et al.[16] developed a crack identification technique using an

integrated active piezoelectric sensor network in aluminum plates. Li et al.[17] also developed a quantitative damage image identification technique using a circular PZT's array where it is used to construct damage images using the acquired Lamb wave signals. On the other hand, SHM is used in anisotropic materials, that have properties that vary with direction, such as composites to detect air bubbles, voids, blisters, fiber misalignment or wrinkling, fiber failure, matrix crazing and cracking, resin-rich or poor sites, layer separation or delamination. Also, bond failures, crushing of cores, core shear, externally visible or internal impact damage, and other aspects that could result in long term deterioration[3]. Doh Roh et al.[32] proposed analytical and experimental methods to predict and detect deformation and inter-laminar crack propagation in carbon-fiber-reinforced plastics based on electrical resistance measurement where they investigate the electromechanical behavior of CFRP from the elastic region to crack propagation.

SHM systems alone cannot ensure a higher level of safety or better methods of maintenance, however, they can reduce the number of unnecessary inspections and tracks the deterioration, capacity, and remaining service life[3]. Many challenges are still faced in SHM technology such as transferring the technology work tasks to a real practical environment. For guided waves, it is difficult to obtain accurate input parameters that affect the modeling accuracy. Also, it is difficult to interpret the obtained signal due to the multimode propagation, mode conversion, and boundary reflections in complex geometries. Besides, the effect of the environment on the sensor such as temperature, humidity, high stress, mechanical vibrations, shocks, and radiations in addition to challenges related to adhesive bonding used to mount the sensor to the material. SHM for composite materials has additional challenges dealing

with the anisotropy and wave velocity. The anisotropy, viscoelasticity, and inhomogeneity also affect the propagation power. Besides, it is difficult to differentiate critical composite damage such as delamination defects from structural variability during fabrication. Finally, the study of guided waves in composites of unknown material properties[11]. That is why these systems are still being investigated to overcome the challenges, increase their performance, and increase their usage in different fields.

B. Guided Waves

Guided waves are elastic waves propagating between two parallel plates with free plane surfaces[33], they can also propagate in thin plates, tubes, rods, and multilayered structures[11]. They propagate for long distances covering the total thickness of the structure [11]. These waves are divided into different waves mainly: Rayleigh, Lamb, and Stoneley waves. Rayleigh waves are guided waves that propagate over the surface of a very thick structure also known as a semi-infinite object. For those waves to be generated the wavelength should be very small compared to the thickness, and these waves decay with depth[11]. Lamb waves are guided waves propagating in two thin parallel free surfaces, where the plate thickness becomes comparable to the wavelength[33, 34]. They are waves of plane strain that occur in a free plate[11]. Finally, Stoneley waves or Rayleigh-like waves are guided waves that propagate at the boundary joining two semi-infinite solids for a suitable choice of material[11, 33].

Guided waves have been used as primary methods to detect damage in materials and they become an important aspect in the SHM systems. Different papers discussed the usage of lamb waves in their research, where Philibert et al. [9] designed a sensing

method to assess damage in a Composite T-Joint using guided waves. Memmolo et al. [35] detect, localize, and assess the size of disbanding in a stiffened composite material. Nazeer et al.[19] studied the interaction of guided waves with a bend region in anisotropic material and how these waves are affected by the bend curvature.

These waves are multimodal where a single wave can split into different modes, and their wave shape changes while propagating which makes them dispersive [36]. Xu et al. [37] proposed a signal mode and multi-mode dispersion compensation processing method where they built a dispersion signal dictionary by utilizing the dispersion curves to decompose the recorded waves. Xu and Ta [38] proposed a mode separation method that compresses the individual dispersive waveforms into temporal pulses which makes the signal un-overlapped with time and frequency so the modes can be extracted. Multimode and dispersion affect the signal analysis in addition to instrumentation, ambient noises, and the operational conditions which makes the analysis challenging. Due to the lack of freely available standard measurements to comparatively evaluate existing methods Moll et al.[39] introduced the “Open Guided Waves” an extendable online platform that provides highly qualified and documented datasets for inspection using guided waves.

According to Dr. Rose[11], ultrasonic guided wave techniques have many advantages. First, it can inspect long distances from a single probe where all the data can be acquired. Second, Guided waves have great sensitivity which provides a better image of the material’s health. Third, it allows the inspection of hidden structures, coated structures, structures below water, structures running in soil, and structures encapsulated in concrete. Fourth, the inspection is simple and rapid so they are cost-effective.

Guided waves are now being enormously used for both SHM and NDT and their usage exploded due to the increasing understanding and the significant advances in computational power.

C. Damage Detection Methods

Damage is the change that affects a body's performance, it is usually noticed by comparing the body with an initial state which is the undamaged[28]. These changes include a change in the material, geometric properties, boundary conditions, and system connectivity. The Damage starts at the material level might not be always a concern, but it starts to grow under loading scenarios to affect the material functionality[28].

The vibration-Based Techniques monitor changes in the model frequency and involves the entire frequency with its boundary conditions where damage can be indicated based on reflection and mode conversion phenomena[30]. A guided wave-based SHM technique has different advantages: they are cheap, light-weight, and easily included in the structure, they are capable of scanning large areas with a small number of transducers, they can implicate a range of frequencies from low to high so they can detect both large and small damage.[36]

Damage detection starts as early as the fabrication process and continues after putting the equipment in use. Chandarana et al. [40] monitor the development of strain in-situ of the resin infusion process during a composite fabrication process. Pieczonka et al [10] used a mode-converted lamb wave to detect damage in composite panels. The method is based on the difference in amplitude and group velocity between the symmetric and antisymmetric Lamb wave modes during vibration when comparing the in-plane and out-of-plane wave vector component, so wave modes can be detected. In

aircraft, the automated inspection systems are used to cover various inspection types. Local inspection techniques focus on specific damage of a known appearance while the global technique is used to inspect relatively large areas and aim in locating suspected positions that will be then scanned by special inspection techniques. For both local and global aircraft, automated inspection systems static and dynamic techniques are utilized. The dynamic techniques are continuously active to monitors the emitted signal during the damage propagation process resulting from impact events or in-service loads, while the static technique measures the state of damage at the moment of recording[23].

D. Signal Processing Techniques

The obtained signals are usually complex due to noise, environmental variation, multiple wave modes, and multiple reflections from boundaries, therefore data processing is required to analyze these signals[36]. The processing of these signals helps in de-noising, data compression, feature extraction, and damage index formulation. The commonly used technique is the time-frequency analysis such as the waveform transform that decomposes a time signal into frequency band components[41]. However, it has a drawback in the analysis of dynamic responses[36].

The Fourier Transforms is a simple way that is also used for processing guided waves and includes the short term Fourier Transform (STFT), continuous Fourier transform (CFT), in addition to Integral transform, Hilbert transform, Hilbert-Huang transform, and Wigner-Ville distribution[30, 36]. Alleyne and Cawley[42] presented a method that involves a two dimensional Fourier transformation of the wave received time history at a series of equal space positions along the propagation path that measures and analyzes the propagating multimode signals.

Matching pursuit(MP) has recently been used where the signal is decomposed into a linear combination of waveforms from a redundant dictionary[36]. Kim and Yuan [7] proposed a damage localization image algorithm where they used the MP algorithm for separating wave packets individually.

Other processing techniques use Frequency-wavenumber domain analysis. Michaels et al[43] and Ruzzene[44] used the Frequency-wavenumber analysis to separate the wave modes and remove source waves from a wave field data that is rich with information regarding the space and the time variation of propagating waves in damaged structural components.

CHAPTER III

EXPERIMENTAL AND NUMERICAL METHODOLOGIES

A. Lamb waves

Lamb waves are known for their presence in thin solid plates. Mathematical physicist, Horace Lamb, first described these waves in 1917 as elastic waves [45] causing particles to move in- and out-of-plane (parallel and normal) with respect to the direction of propagation. These waves travel across the plate by reflecting off the upper and lower boundaries of thin-like structures. Two sets of infinite Lamb wave modes are thus generated making the properties of these waves very complex. These waves are multimodal where the signal input splits into different wave modes[36]. In the last two decades, the increase of computational method capabilities allowed researchers to understand Lamb waves better and their usage thus increased in NDT applications.

Lamb waves can be generated using ultrasonic probes, electromagnetic acoustic transducers (EMATs), laser-based ultrasonic, piezoelectric elements (PZTs), air-coupled transducers (ACTs), interdigital transducers, and optical fiber transducers[18, 46]. When the transducer is in direct contact with the material, where the transducer is glued to the area of interest it is called a contact method. Such transducers include the piezoelectric lead zirconate titanate (PZT), MFCs, and fiber optics. On the other hand, Non-contact techniques generate acoustic waves in the material without any direct contact with it. They can be used in a hostile environment, hot or cold materials, in uncured and wet laminates, and in geometrically difficult to reach locations[47]. Such methods include ACTs, EMATs, laser generation, and optical holographic. By combining one or two of the mentioned devices, different contact and noncontact methods could be formed.

Contact mechanisms require a dense array of data and the usage of many contact transducers, while noncontact mechanisms provide an easy scan for the region of interest without the need for any coupling [48].

1. Fundamentals of Lamb Waves

Lamb waves are dispersive waves, which means that the wave velocity varies with the frequency and the plate's thickness. The lamb waves generate different wave modes anti-symmetric A_i where $i=0, 1, 2, 3$, etc. and symmetric wave modes S_j where $j=0, 1, 2, 3$, etc. The symmetric wave modes have an in-plane direction parallel to the wave propagation direction while the anti-symmetric modes have a particle motion perpendicular to the direction of the wave propagation. Harb and Yuan[13] discussed that Lamb waves can be effectively modeled by using traction-free surface boundary conditions on the equation of motion and that introduces the dispersion phenomenon. This phenomenon for a plate placed in a vacuum bounded by surface layers $z = \pm \frac{h}{2}$ where h is the plate thickness and extended infinitely in both the x and y directions for a linear, homogenous and the isotropic elastic plate is

$$\frac{\omega^4}{C_T^4} = 4k^2 q^2 \left[1 - \frac{p \tan\left(\frac{ph}{2} + \gamma\right)}{q \tan\left(\frac{qh}{2} + \gamma\right)} \right] \quad (1)$$

where γ represent the symmetric (S) and antisymmetric (A) lamb wave modes for values 0 and $\frac{\pi}{2}$ respectively.

$$p^2 = \frac{\omega^2}{C_L^2} - k^2 \quad \text{and} \quad (2)$$

$$q^2 = \frac{\omega^2}{C_T^2} - k^2 \quad (3)$$

where k is the wavenumber, ω is the angular frequency, C_L and C_T are respectively the longitudinal and transverse velocities of the bulk material.

2. Dispersion Curves in Aluminum 1050

Lamb waves are highly dispersive that is the wave shape changes as it propagates. Lamb waves speed depends on the frequency f and half the speed thickness z , the variation of wave speed with the frequency produces the dispersion[29]. The dispersion curves, Figure 1, and tuning curves, Figure 2, were obtained experimentally by varying the frequency from 50 to 350 kHz with an increment of 10 kHz and theoretically using the Wavescope Software[49] by calculating the speed and the amplitude for each mode respectively.

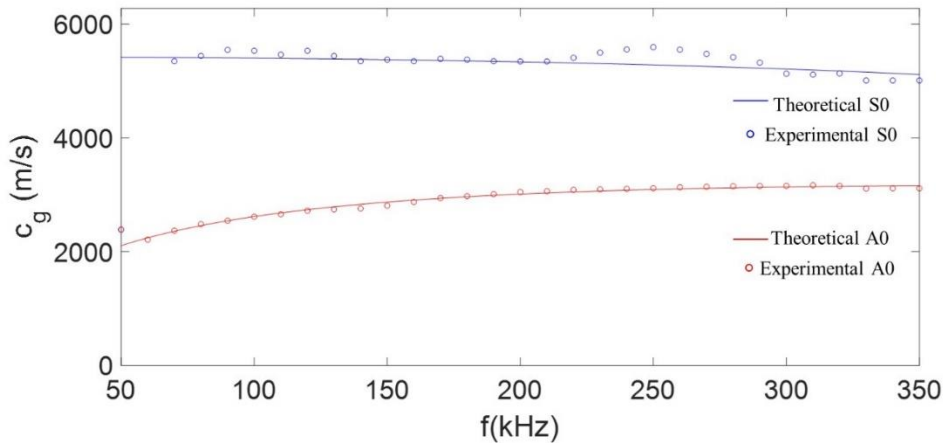


Figure 1. Group velocity dispersion curves for 3mm thick aluminum 1050.

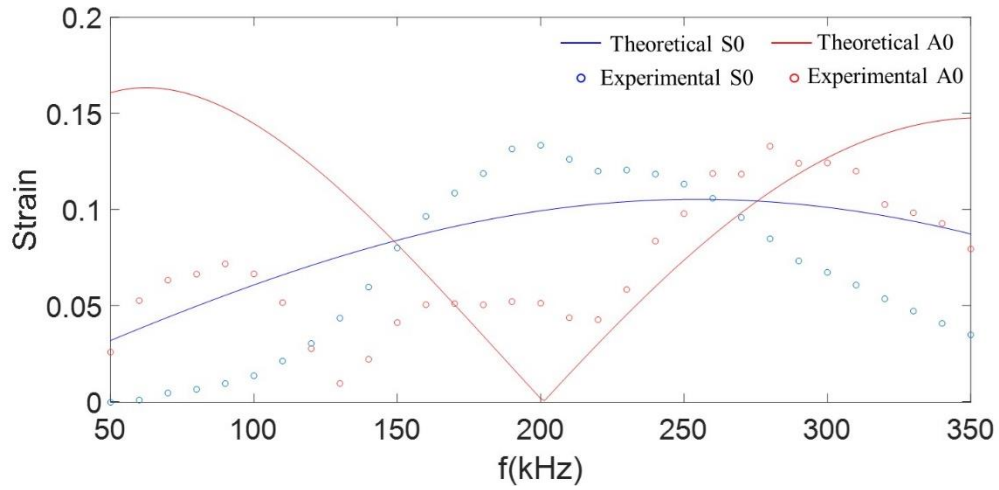


Figure 2. Amplitude tuning curves for 3mm thick aluminum 1

A. Signal Used

A low bandwidth five-cycle Hanning windowed tone-burst signal is used in the experiment for 100 kHz and 200 kHz frequencies. Figure 3 and Figure 4 (a) shows the signal with its envelope, and (b) shows the frequency spectrum for 100 and 200 kHz respectively.

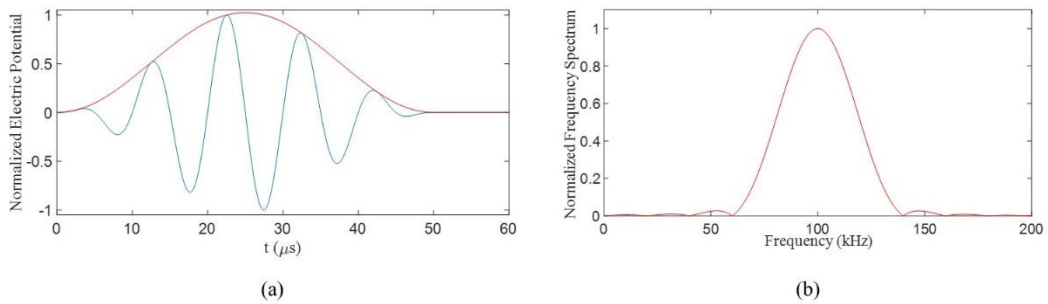


Figure 3. (a) Five-peaked Hann-windowed tone-burst signal at 100kHz center frequency, (b) its frequency spectrum

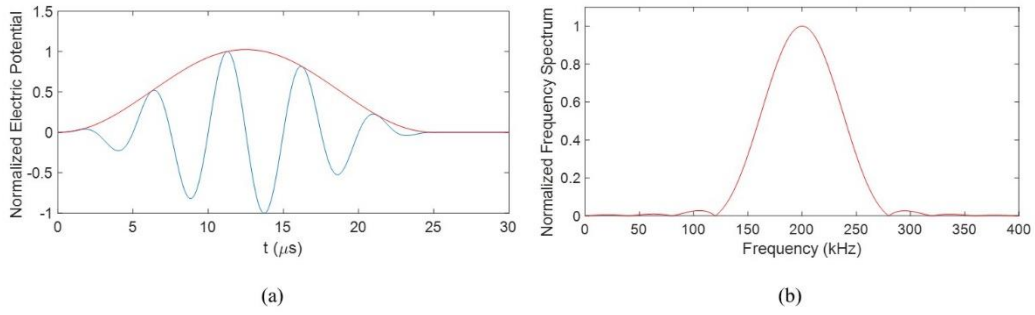


Figure 4. (a) Five-peaked Hann-windowed tone-burst signal at 200kHz center frequency, (b) its frequency spectrum

B. Experimental Setup

A Keysight 33500B signal generator was used to generate the low bandwidth five-cycle signal which was fed into a broadband linear amplifier (Piezo System Inc. EPA-104) to overcome Lamb wave attenuation. The amplified signal plotted in Figure 3 and Figure 4 was then applied to the PZT discs. Upon excitation, Lamb waves were generated in the plate which was then measured by the other PZT sensors for this experiment as shown in Figure 5 and by an Optomet Laser Doppler vibrometer (LDV) for the second experiment as shown in Figure 6 and recorded using a Keysight InfiniiVision DSO-X 3024A digital storage oscilloscope. Two experiments were done on a 3 mm thick aluminum 1050 plates with the following properties: $E=71\text{ GPa}$, $\nu = 0.33$, and $\rho = 2710\text{ kg/m}^3$.

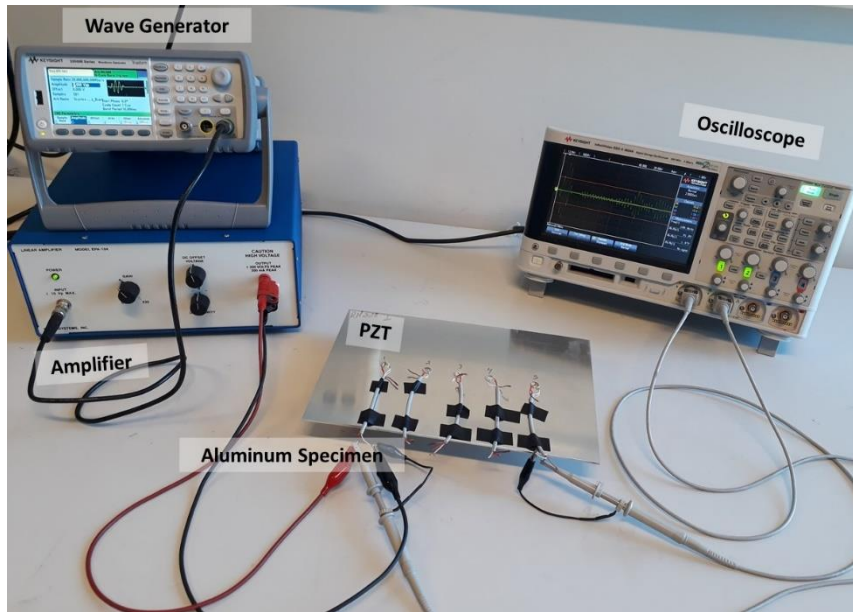


Figure 5. Experiment setup for the experiment of a perpendicular bent on lamb waves in an aluminum plate

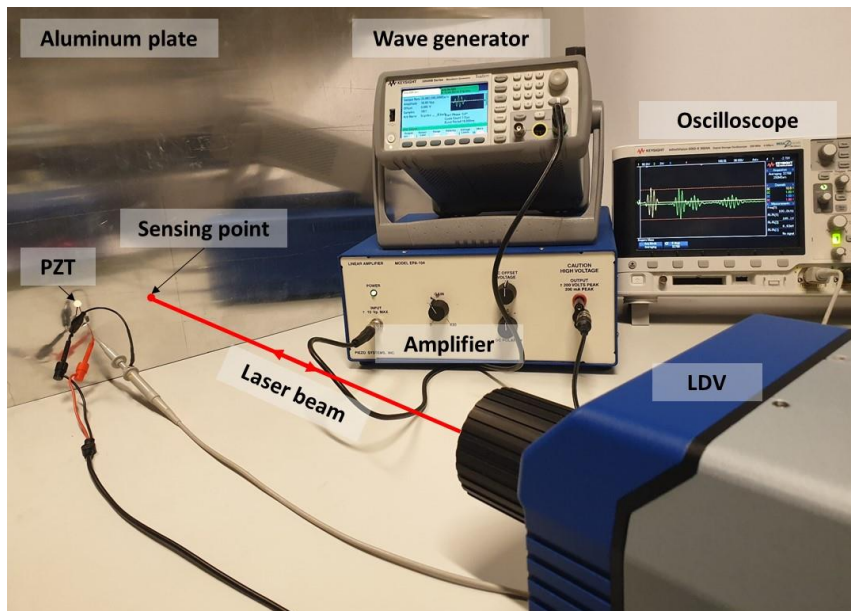


Figure 6. Experiment setup for the study of boundary reflection and attenuation

1. Effect of a perpendicular bent on lamb waves in an aluminum plate

This experiment was conducted on three aluminum plates of different sizes and geometries, as shown in Figure 7. A set of five circular PZTs, each having a dimension of 10 mm diameter and 1 mm thickness, was bonded to the surface of each plate along the horizontal line of symmetry as shown in the same figure in a pitch-catch configuration. In each of the three plates, PZT 2 from the left side of the plate acted as an actuator while PZT 5 measured the propagating wave. The computed signals at each frequency (100 and 200 kHz) were then recorded and plotted against each other. Data from Waveform Revealer[50] were treated as baseline signals since it does not account for any reflections nor attenuation from the material and present PZTs. Plate 1 was studied to understand the reflections from free-edge boundaries while data from Plates 2 and 3 were used to characterize reflected waves on bent edges in metallic plate-like structures.

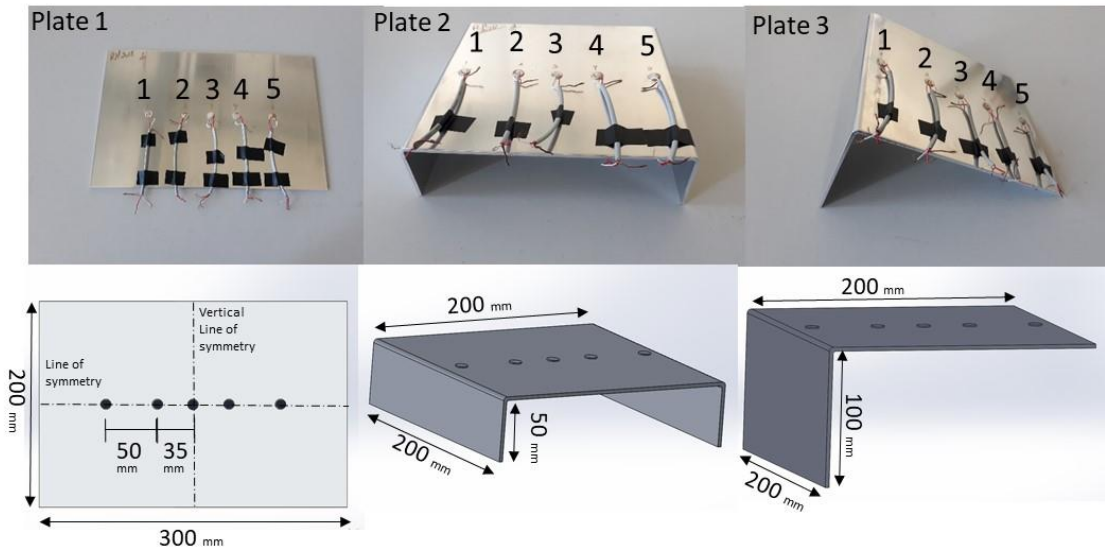


Figure 7. Actual and modelled Aluminum 1050 plates

2. The study of boundary reflection and attenuation of lamb waves in an aluminum plate

This experiment was conducted on two aluminum plates, plate L ($1m \times 1m \times 0.003m$) and plate S ($0.3m \times 0.2m \times 0.003m$) as shown in Figure 8. A set of PZTs, each having a dimension of 7 mm in diameter and 0.2 mm in thickness, were bonded to the surface of those plates in a way that the reflection of the boundaries can be detected when comparing these plates. PZT A is placed in region 1 far away from all edges to eliminate boundary reflections, PZT B is placed in region 2 at a distance from the top equal to that of plate S and far away from all other sides to obtain the top reflection only, and PZT C is placed in region 3 in a position similar to that of plate S from the corner and away from the top and right boundaries to obtain reflections from the left and the bottom edge as shown in the same Figure.

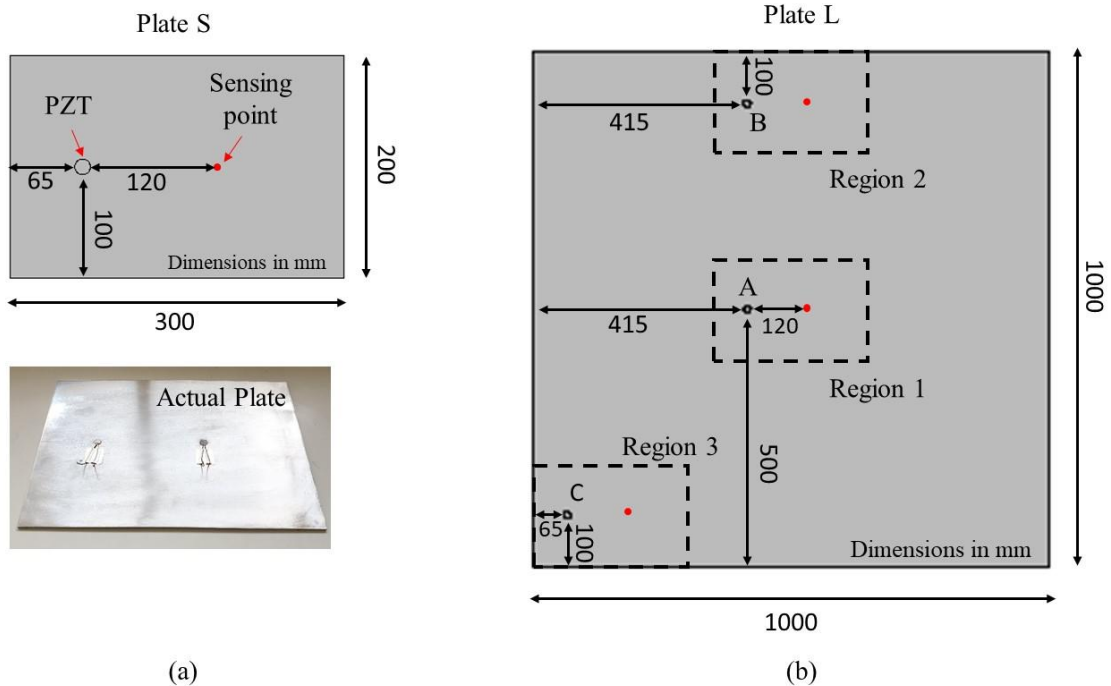


Figure 8. Aluminum specimens used and PZTs placement configuration

3. Effect of the angle of the bent on lamb wave in an aluminum plate

This experiment was conducted on plate S. Two PZTs, each having a dimension of 7 mm in diameter and 0.2 mm in thickness, were bonded to the surface in the middle of the plate at a distance of 115 mm and 235 mm from the edge. Two-line scans regions were taken, Line 1 and line 2 were taken at a distance of 198 mm and 202 mm parallel to the left edge respectively as shown in Figure 9

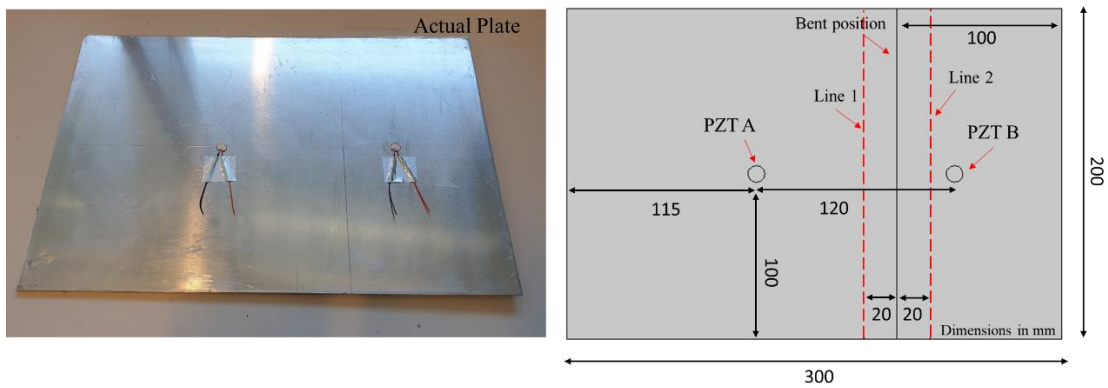


Figure 9 Aluminum 1050 plate S showing the location of the line scans and the bent

The plate had been bent an increment of 30 *degree* ranging from 0 to 150 *degree* as shown in **Figure 10** after collecting the required data for each angle.

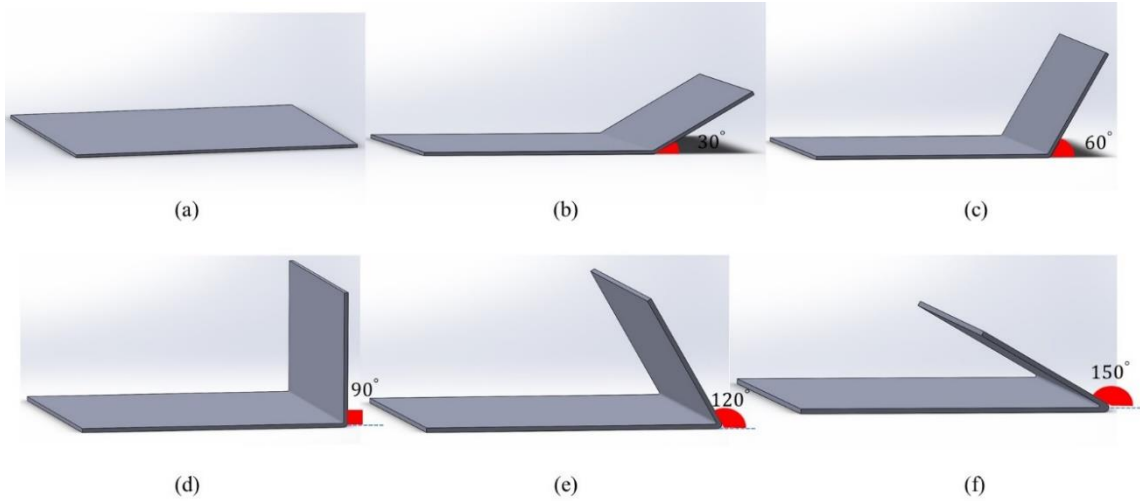


Figure 10 Aluminum specimen used with the variation of bent angle

C. The Chosen Frequencies

Based on the theoretical group velocity dispersion curve shown in Figure 1 and the amplitude tuning curve found experimentally and using Wavescope Software [49] shown in Figure 2, the magnitudes of the firstly arrived A_0 and S_0 waves were compared to each other with respect to the center frequency of the excited waves. It was found that at around 90 kHz the A_0 reached high amplitude when compared to S_0 while at 200 kHz the S_0 mode reached a maximum where A_0 was diminished. Based on this result and for the ease of the experiments, the chosen frequencies for our study were 100 kHz and 200 kHz. Both experiments were performed using those frequencies.

D. The Numerical models

1. Effect of a perpendicular bent on lamb waves in an aluminum plate

To analyze and visualize the interaction of Lamb waves with boundaries, a guided wave propagation was emulated based on a three-dimensional (3D) finite

element software, COMSOL Multiphysics was used for this analysis. The plates and PZTs used in the experiments were 3D modeled using the Structural Mechanics Module with Piezoelectric Solid Interaction physics. The material of the plate and PZT discs were chosen as Al-1050 and PZT-5H, respectively.

The actuating PZT discs attached to the plates were actuated by the same input signal generated by the wave generator in the experiment section. The amplitude was modified to match the experimental input amplitude so that the results can be easily compared. The signal was applied to the PZT face as an electrical potential.

2. The Mesh

The geometry of each plate was divided into three different regions as shown in Figure 11. Most of the plate was considered to have quadrilateral elements that were mapped and swept to have an optimum computational time; since these cubic elements have the best quality at a lower number of elements. The PZTs had to be taken as free tetrahedral elements since they are considered as complex geometries. Hence, the region between the two had to have nodes that match both previous regions, which is why it was specified as triangular elements to bond with the tetrahedral elements above it and swept into prism elements within the thickness to bond with the hexahedral elements next to it.

Table 1 Maximum element size and number of elements

	r	Δx_{max} (mm)	Elements
Mesh 1	10	1.551	99165
Mesh 2	12	1.292	134080
Mesh 3	14	1.107	178105
Mesh 4	15	1.034	202816
Mesh 5	16	0.968	228197
Mesh 6	17	0.912	256669
Mesh 7	20	0.775	353236

One of the most significant parameters in the implementation of COMSOL is the mesh density. Increasing the density improves the accuracy, but increases the computational complexity of the model. Different maximum element sizes were tested to choose the optimal mesh density as presented in Table 1. In the case of wave characterization, the maximum element size (Δx_{max}) should be chosen following the wavelength of the excited wave (λ) according to the equation

$$\Delta x_{max} = \lambda/r \quad (4)$$

where $r = 1, 2, 3, n$ is the wavelength-element size ratio. The wavelength was calculated based on the following equation

$$\lambda = v/f \quad (5)$$

where v is the excited wave phase velocity in (m/s) and f is the frequency of excitation in (kHz). For an excitation wave of 100 kHz center frequency, the wavelength was

$$\lambda_{100} = \frac{v}{f} = \frac{1551m/s}{100\text{ kHz}} = 15.51\text{ mm}. \quad (6)$$

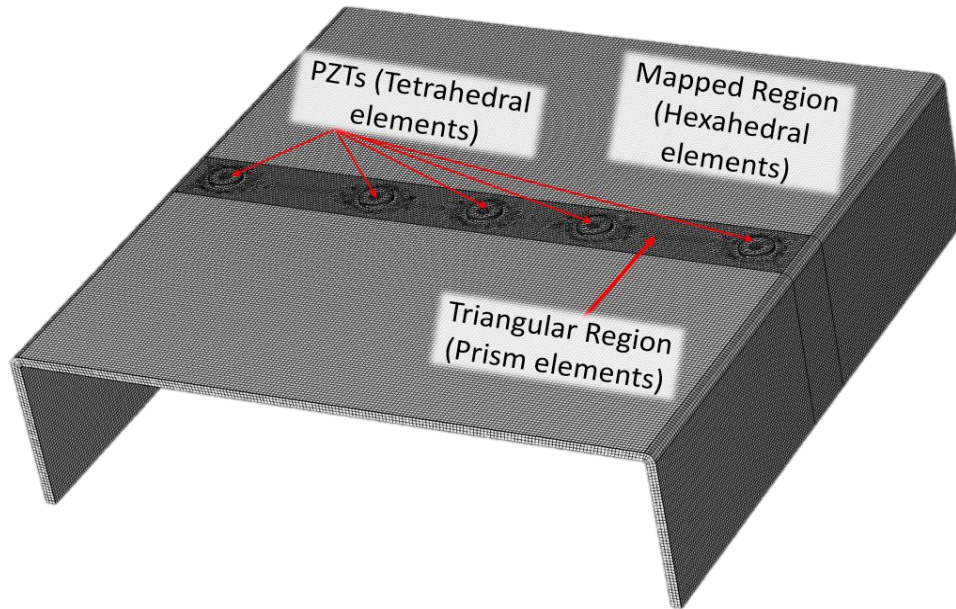


Figure 11 Mesh plot and meshed regions of Plate 2 in COMSOL model

According to the obtained results, it has been realized that the data was varying as the wavelength-element size ratio varied between 10 and 20. It is known that the element size and the computational time are inversely proportional and based on the results, the chosen mesh was of ratio 15 which resulted in an acceptable steady solution. Also, the time step used in the COMSOL model was 2.5×10^{-7} sec which is far below the reported value used in the literature [51].

3. The study of boundary reflection and attenuation of lamb waves in an aluminum plate

ABAQUS and COMSOL Multiphysics finite element software were used to better analyze and visualize the interactions of Lamb waves with the edge boundaries in 3D. The aluminum 1050 plate S was modeled with the same dimensions as shown in Figure 8 and the same material properties are given earlier. A concentrated point load was placed at the center position of the PZT and was used to actuate the plate by the

same input signal generated by the wave generator in the experiment section. Another point at a distance of 120 *mm* was placed on the surface of the plate to measure the propagating wave and detected as an out-of-plane velocity signal. The mesh used was a quadrilateral element mesh that was mapped and swept over the entire plate as shown in **Error! Reference source not found.**a with an average element quality of 0.98. Its density was chosen according to the recommended one-tenth value of the wavelength λ based on equation 5[51]. Also, the step time used for the simulation was 1×10^{-7} s.

In COMSOL Multiphysics both the plate S and the PZT used in the experiments were 3D modeled using Structural Mechanics Module with Piezoelectric Solid Interaction physics. The material of the plate and PZT discs were chosen as Al-1050 and PZT-5H, respectively. The actuating PZT discs attached to the plates were actuated by the same input signal. The amplitude, however, was modified to match the experimental input amplitude so that the results can be easily compared. The signal was applied to the PZT face as an electrical potential. The plate's geometry was divided into three different regions as shown in Figure 12b for a more consistent mesh. The largest portion of the plate is meshed using quadrilateral elements that were mapped and swept. The PZTs are considered as complex geometries, thus they had to be taken as free tetrahedral elements. The mesh density used is the same as that used in the ABAQUS model. Besides, the time step used in the *COMSOL* model was 2.5×10^{-7} s .

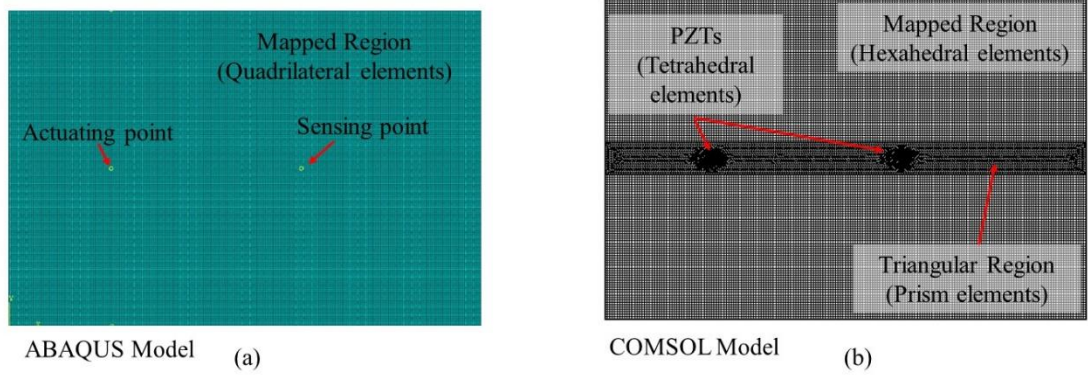


Figure 12. ABAQUS and COMSOL FEA meshed models for plate S

CHAPTER IV

LAMB WAVE MODES AND BOUNDARY REFLECTION DETECTION

Different signals measured experimentally using the LDV and a PZT were recorded and compared to theoretically predicted signals from Waveform Revealer [50] as shown in Figure 13a and 11b for 100 and 200 kHz , respectively. The theoretical signal predicted using Waveform Revealer is based on the diameter of the actuating and receiving PZTs, separation distance, plate thickness, and material properties. Then the wave envelopes of each signal were drawn as shown in Figure 13c and 11d. The wave envelope is formed by finding the absolute value of the signal and then tracing the peaks obtained to form the given shape.

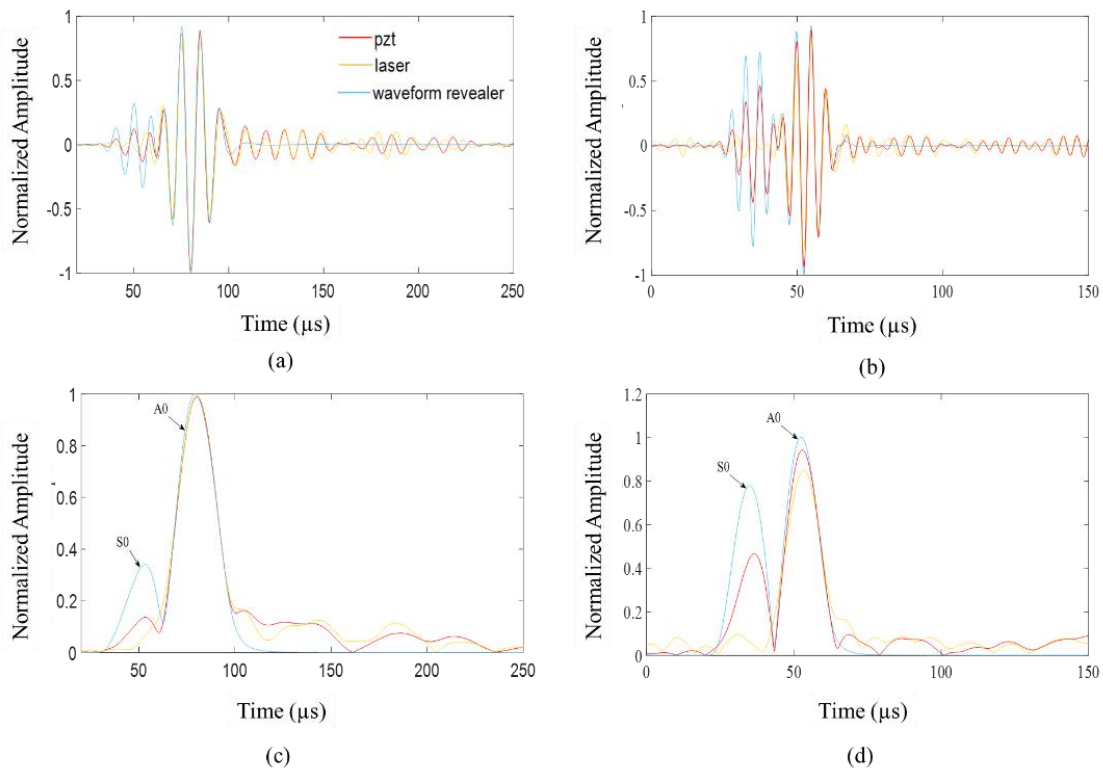


Figure 13. Experimental (PZT and LDV) and theoretical captured signals at (a) 100 kHz and (b) 200 kHz , with their respective envelopes in (c) and (d).

By comparing the experimental results of plate L using the LDV to that of the PZT and the Waveform Revealer signal, it is noticed that the normalized signals were very close in both central frequencies. The arrival time of each mode was then calculated where the traveled distance is known and the velocity of each mode is obtained from the dispersion curves in Figure 1. This shows that packet one and two were the S0 and A0 modes, respectively. The A0 mode was sensed by both the PZT and the laser for both frequencies shown in Figure 13. On the other hand, the S0 mode was only detected by the PZT with an amplitude lower than the numerical value obtained by the Waveform Revealer, but it was not detected by the laser since it measures the dominant out-of-plane vibration.

In this work, boundary reflections have been detected and investigated experimentally by generating and measuring the fundamental Lamb waves modes (A0 and S0) at low frequencies (100 and 200 *kHz*) in the small dimensional plate S and the three separate regions (1, 2, and 3) of plate L as shown in Figure 8. The separation distance between the excitation and receiving points in all four cases was kept at 120 *mm*. The LDV measured signals from these cases and at an excitation frequency of 100 *kHz* were plotted in Figure 7 where the first arrival for A0 mode and the reflections from different edges were easily detected. Figure 14a shows the dominant incident A0 mode recorded at 50 μ s in region 1 of plate L without any major reflections. Region 1 being in the middle of the plate is far enough from any edge of the plate for the reflected waves to be detected. The detected Lamb wave in region 2 of plate L is plotted in Figure 14b showing the first incident A0 mode as the first envelope and a new envelope detected at around 90 μ s which represents the reflected wave of A0 mode from the top edge of the plate. The Lamb wave signal in region 3, plotted in Figure 14c, shows an

additional envelope that appears around 140 μ s resulting from the reflection of A0 mode from the left edge and left bottom corner of plate L. Reflections from all boundaries could be noticed in the measured signal of plate S as plotted in Figure 14d. Similar graphs were plotted at an excitation frequency of 200 kHz as shown in Figure 15. By comparing the measured data from the three regions of plate L with that of plate S at 100 and 200 kHz frequencies, the four edges and corner boundary reflections can be easily identified.

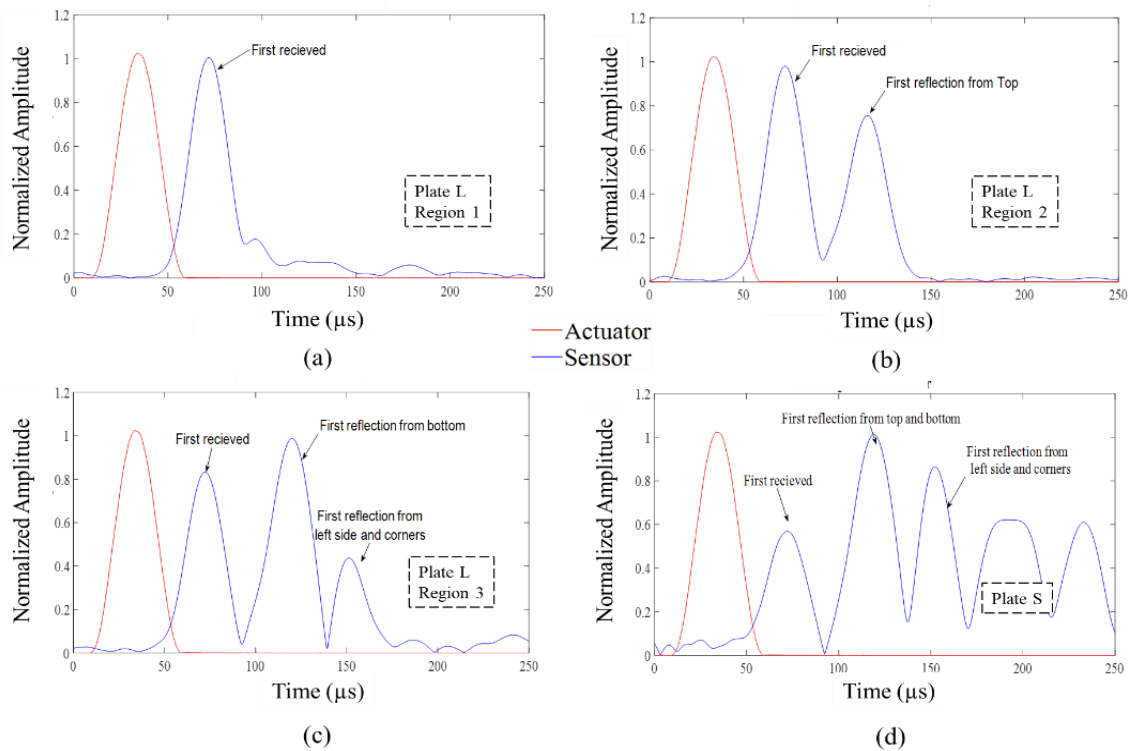


Figure 14. LDV measurements at 120 mm from the actuators in plates L and S at 100 kHz excitation frequency.

The time of arrival and the amplitude of the reflected waves could be directly used to identify the intensity of reflection as well as the separation distance between each edge and the excitation and receiving points. For instance, the intensity of the first reflection in plate S is higher than that of the first arrival of the A0 mode due to the

superposition of the reflections of the upper and lower boundaries that are symmetric with respect to the sensing point horizontal axis.

Both ABAQUS and COMSOL models provide a clear wavefield for the generated Lamb waves at 200 kHz in plate S as shown in Figure 16. The first wave field snapshot at 50μs shows the arrival of the first incident wave at the sensing point. The snapshot at 70μs shows the arrival of the reflected waves from the top, bottom, and left edge to the sensing point. Both wave fields validate the Waveform revealer data shown in Figure 15.

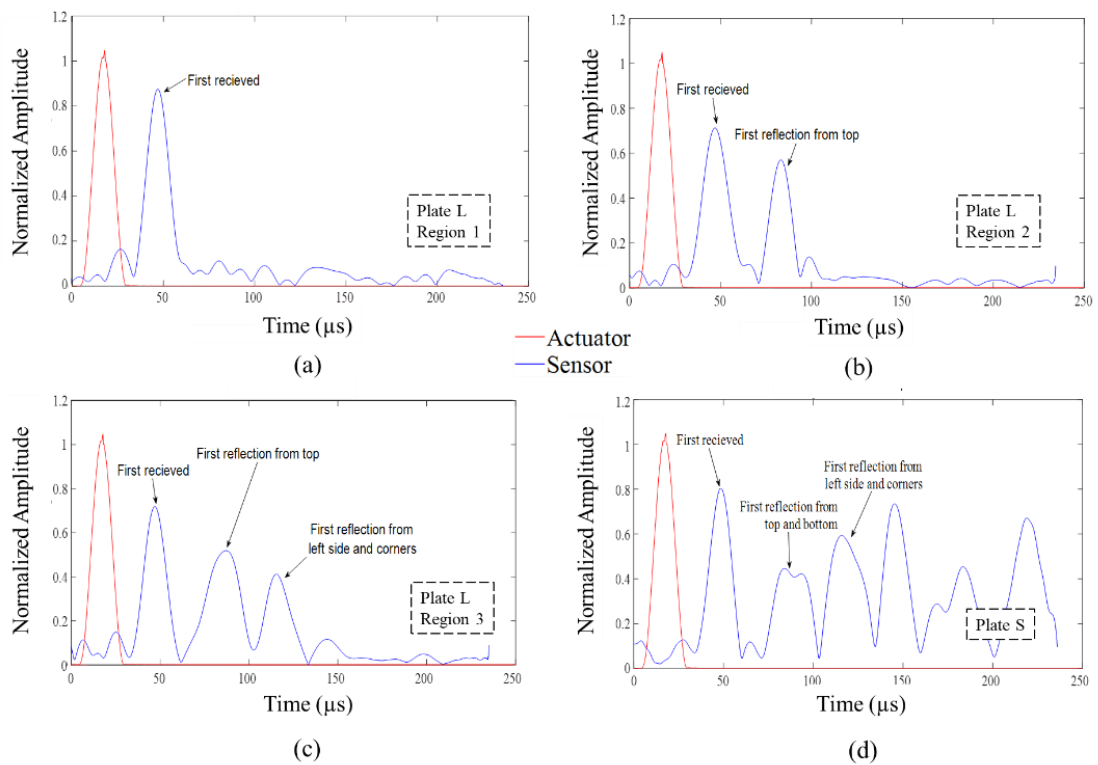


Figure 15. LDV measurements at 120 mm from the actuators in plates L and S at 200 kHz excitation frequency.

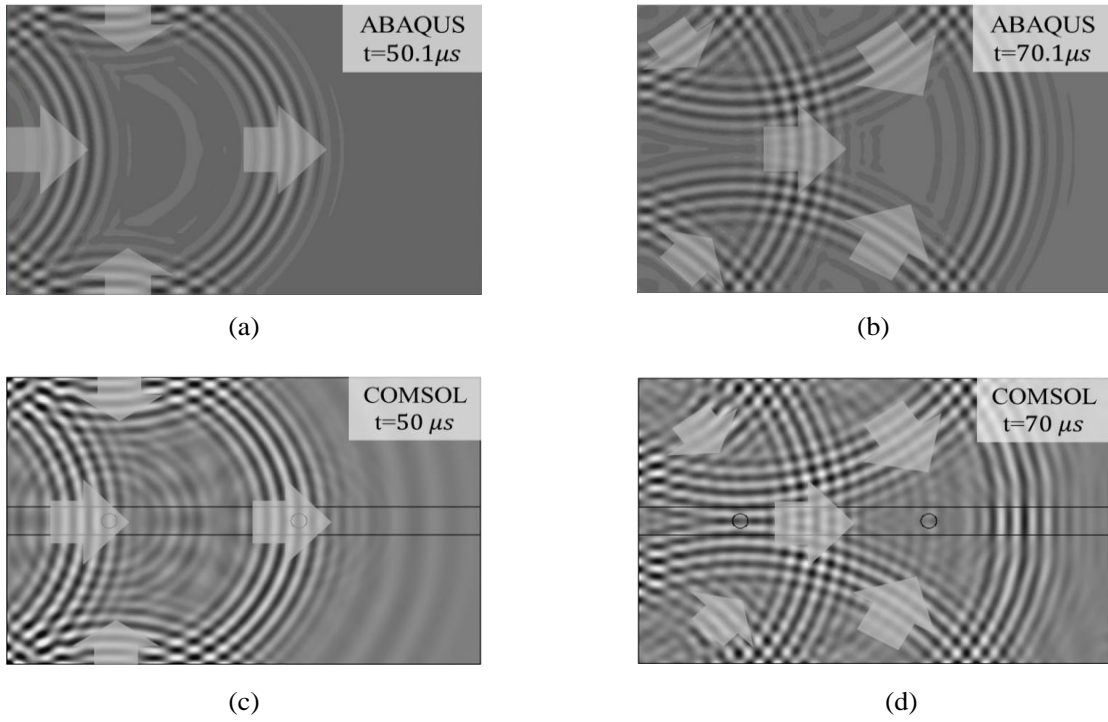


Figure 16. Generated and reflected wavefield (out-of-plane velocity) in plate S at 200 kHz excitation frequency captured from ABAQUS and COMSOL finite element models.

CHAPTER V

LAMB WAVE BOUNDARY REFLECTION THEOREM

Based on Snell's law, the angle of reflection of a propagating Lamb wave is equal to the angle of incidence, since no mode change occurs at the boundary and thus the phase velocity stays constant. This makes it uncomplicated to trace different wave propagating trajectories from the actuator (A) to the sensor (S) after hitting the plate boundary as shown in [11, 15]. The first received signal can be calculated from the time-of-arrival formula

$$v = \frac{d}{t} \tag{7}$$

where v is the velocity in (m/s), d is the distance between the input and output measured in (m), and t is the time needed by the signal to travel the required distance and it is measured in (s).

By analyzing the obtained computational waveform images, boundary reflections, shown as partial circles, could be replicated as waves initially actuated from a virtual point a certain distance away from the boundary of the plate as shown in Figure 17. The boundary reflection theorem aims to find the positions of these virtual actuators. The radius of these virtual circles will be the distance traveled by the wave from actuation until it is sensed after reflection. The time of arrival can be calculated, and the boundary reflections can be assumed.

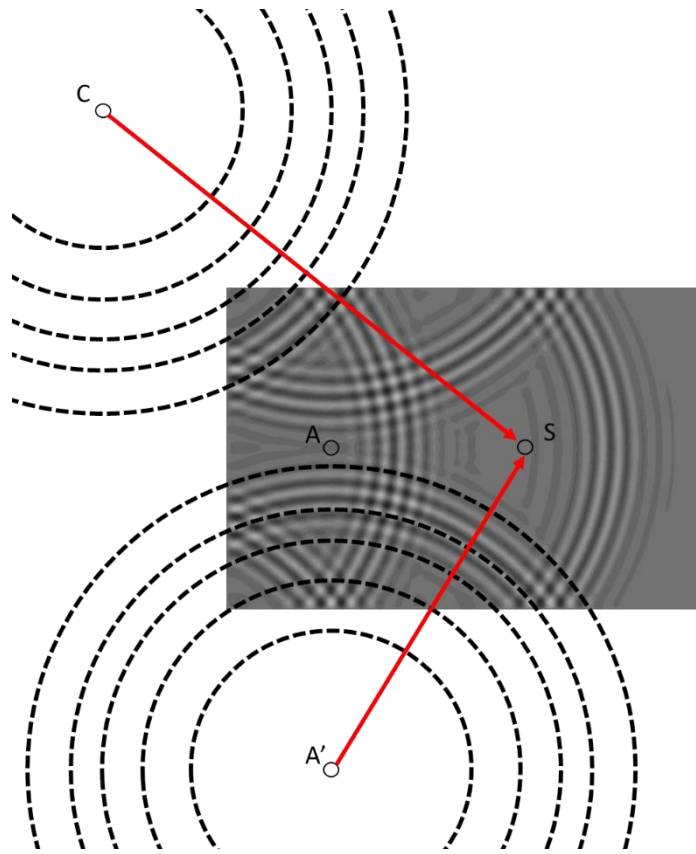


Figure 17. Virtual actuators with the assumed wave propagation.

To simplify this further, the top and bottom edge boundaries of the plate will be focused upon in this case study to explain the proposed boundary reflection theory referred to in Figure 17. A Lamb wave generated by sensor A is first detected as an incident wave by sensor S, then a first reflected wave is detected by the sensor due to the reflection from the bottom boundary reflected from the bottom edge of the plate at point P. A second reflection is measured due to the reflection from point K' from the top edge of the plate after it had reflected from the bottom edge at point K. A third reflection is due to the reflected wave from the bottom edge at point Q'' after it had reflected from the top edge at point Q' and from the bottom edge at Q before that. A large number of reflections are always present in any plate but detected according to the wave's incident energy, attenuation, reflection, and refraction coefficients which are

primarily dependent on the material properties and excited wave. This track will be calculated for the 4 edges following the same pattern so that the whole reflection signal can be built.

The distance covered by the first reflection is equal to the radius of a circle of center A' , a virtual point symmetric to A with respect to the bottom edge, and of radius $[A'S]$. The distance covered by the second reflection is equal to the distance from another virtual point A'' which is symmetric to A' with respect to the top edge as shown in Figure 18. The distance of the third reflection is then the distance from a virtual point A''' symmetric to A'' with respect to the bottom edge and so on. This methodology is repeated for the other sides so that the distance of the other reflections can be determined.

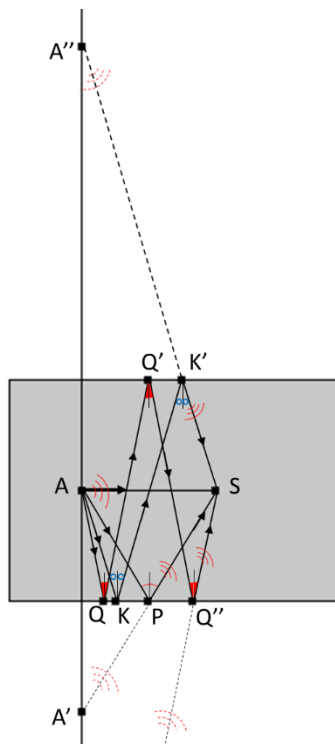


Figure 18. Lamb wave boundary reflection (LBR) theorem sketch.

CHAPTER VI

RESULTS AND DISCUSSION

A. Effect of perpendicular bent on lamb waves in an aluminum plate

Although the experiment was based on two PZTs, an actuator and a sensor, the experimental plates contained five PZTs each. Hence, the COMSOL model was built with additional PZTs to efficiently represent the experimental plates. The absence of the un-used PZTs affected the results obtained as shown in Figure 19. Therefore, for the rest of the numerical simulations, all the PZTs were considered to mimic their effect in the experiments.

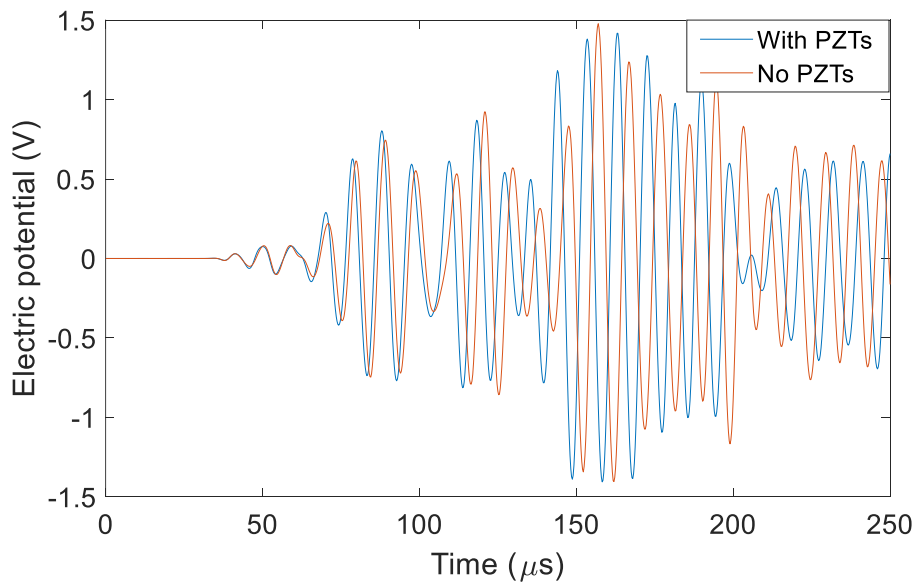


Figure 19. The effect of additional PZT discs placed between actuator and sensor

Two sets of results were obtained for each of the three plates from the two used frequencies. For each plate and at each excitation frequency, the experimental and numerical results were plotted as shown in Figure 20, 19, and 20. In all plates at 100 kHz , the two signals matched to a great extent except for the third packet which as

shown in the figures had a higher amplitude in COMSOL. As for the 200 *kHz* excitation frequency, the results show a good match between the direct incident signals but a variation of amplitudes for the reflected wave packets.

The difference in the third packet at 100 *kHz* from experimental to numerical data is mainly because this reflection passes through all five PZTs while returning from the left to the right side. In reality, damping from PZTs causes more attenuation in the signal and therefore reduces the amplitude of this packet. The same thing could be said for the fourth packet of plate 3 at this frequency. As for the 200 *kHz* frequency, since S_0 was the more dominant mode, and since it has a much higher speed than A_0 , the signal's wavelength is lower, and therefore the effect of the PZTs is even higher in real-life situations. COMSOL might need additional information about the damping of the air around the plate and the glue attached to the PZTs which also causes changes to the sensed signals.

The wave fields of the velocity obtained using COMSOL, in x, y, and z directions representing in- and out-of-plane velocities for the waves, simplified the decomposition of the signal and the packets of the collected signal and their sources can be identified easily. The sensed signal from PZT 5 excited by PZT 2 at 100 *kHz* is plotted in Figure 23. It is noticed that the first packet is a combination of both S_0 and A_0 modes of the first arrived signal. Their out-of-plane wave field (velocity contours in the z-direction) is shown in Figure 24 where S_0 and A_0 are noticed and marked. The second packet is the reflected signal of the A_0 mode from the top, bottom, and right side in addition to a reflected S_0 signal from the left side of the plate. The third packet shows the first reflection of A_0 from the left side of the plate and the fourth packet refers to the second reflection of A_0 from the top and bottom sides. Other reflections from different

angles could also be present but with much smaller amplitudes and could not be seen from any of the plotted wave fields. It is thus noticed that the complexity of measured Lamb waves is due not only to multi-mode excitation but to free-edge reflections in a small plate.

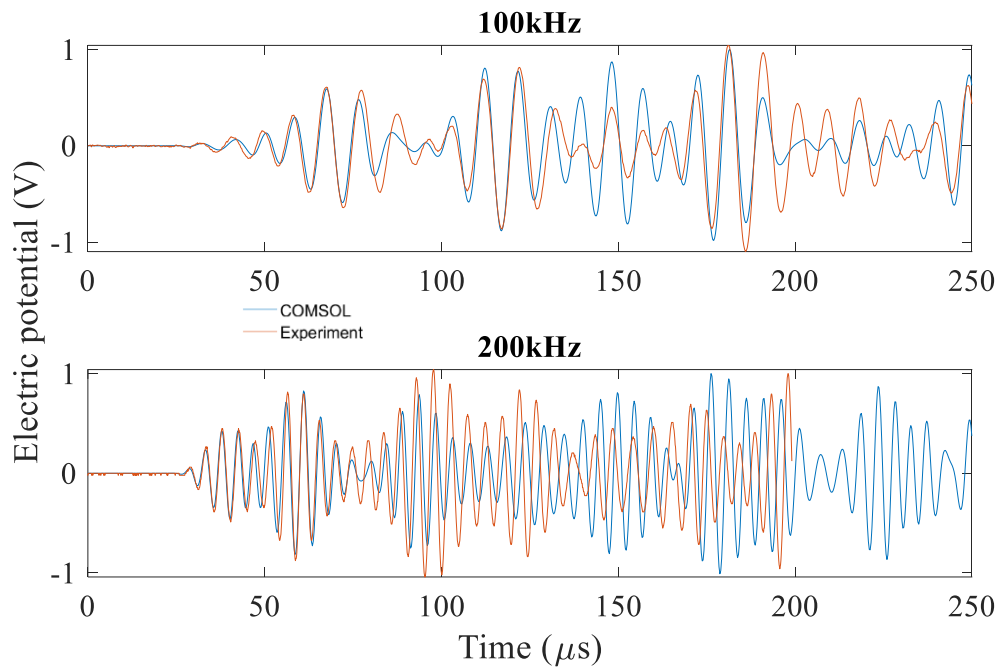


Figure 20. Experimental vs COMSOL results for both frequencies of 100 and 200 kHz for plate 1

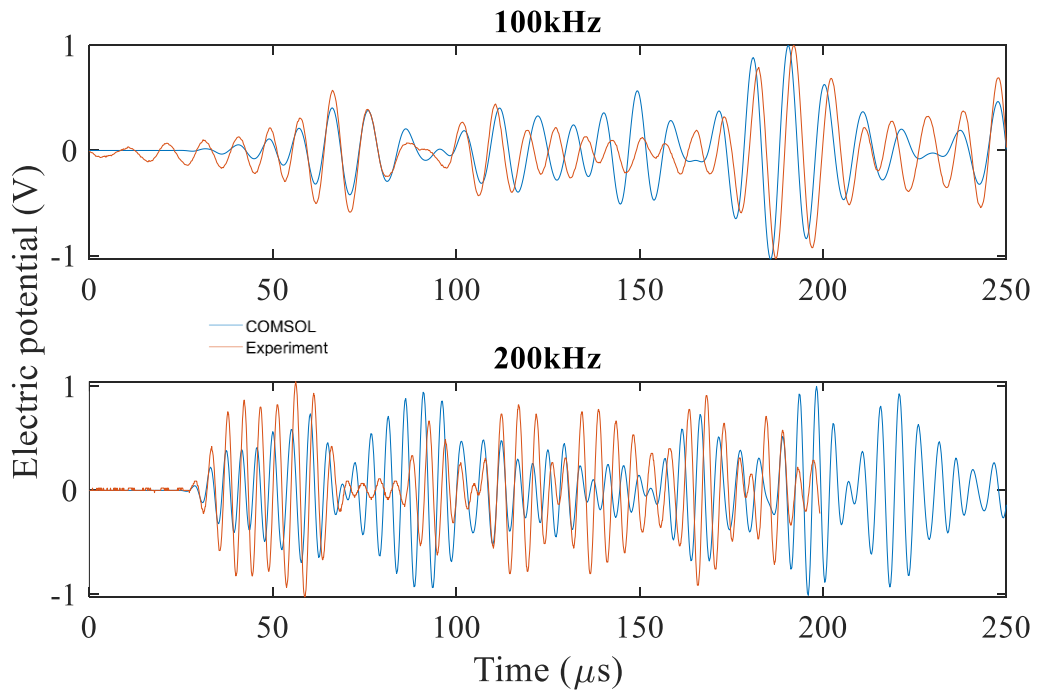


Figure 21. Experimental vs COMSOL results for both frequencies of 100 and 200 kHz for plate 2

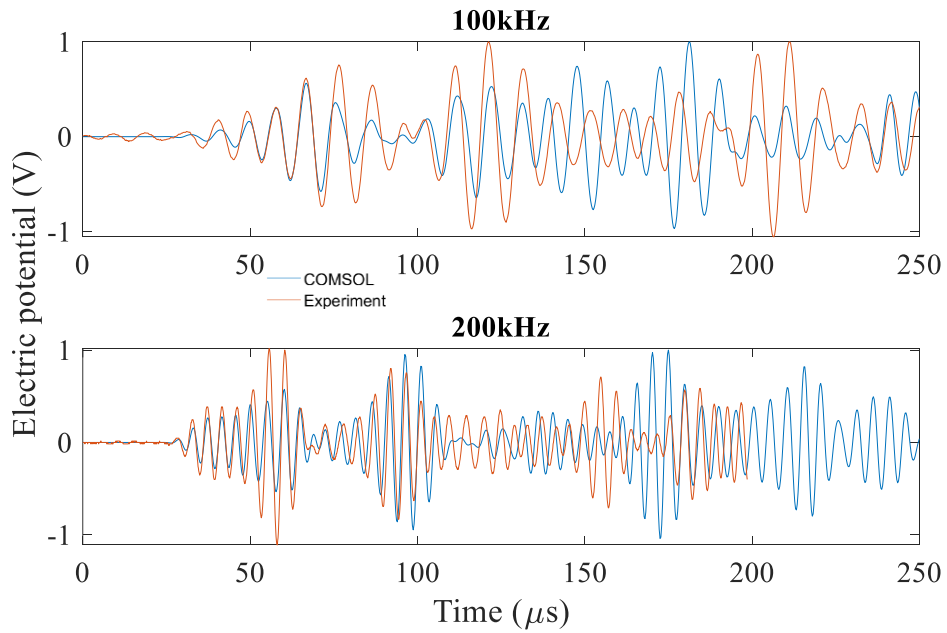


Figure 22. Experimental vs COMSOL results for both frequencies of 100 and 200 kHz for plate 3

To study the effect of the bent edge(s) in plates 2 and 3, the signals obtained from COMSOL at 100 *kHz* excitation frequency were compared to plate 1 to detect their influence on the signal and separate it from the boundary reflections. The wave envelopes in each plate were drawn as shown in Figure 25 and 24. The envelopes matched greatly except for two main time intervals. These intervals are investigated through the wave fields of each plate in the z -direction since A_0 is dominant in this frequency. The second packet or P2 in Figure 26 shows a higher amplitude for plate 1 when compared to the two other plates. The reason behind this difference in amplitude is shown in Figure 27 where the reflection of A_0 from the right bent edge is shown from the wave field of plate 2. This reflected signal diminishes the effect of the transmitted one all the way to the right edge which is full in capacity in plate 1 and makes the amplitude of the right reflection from A_0 at P2 time interval higher in plate 1.

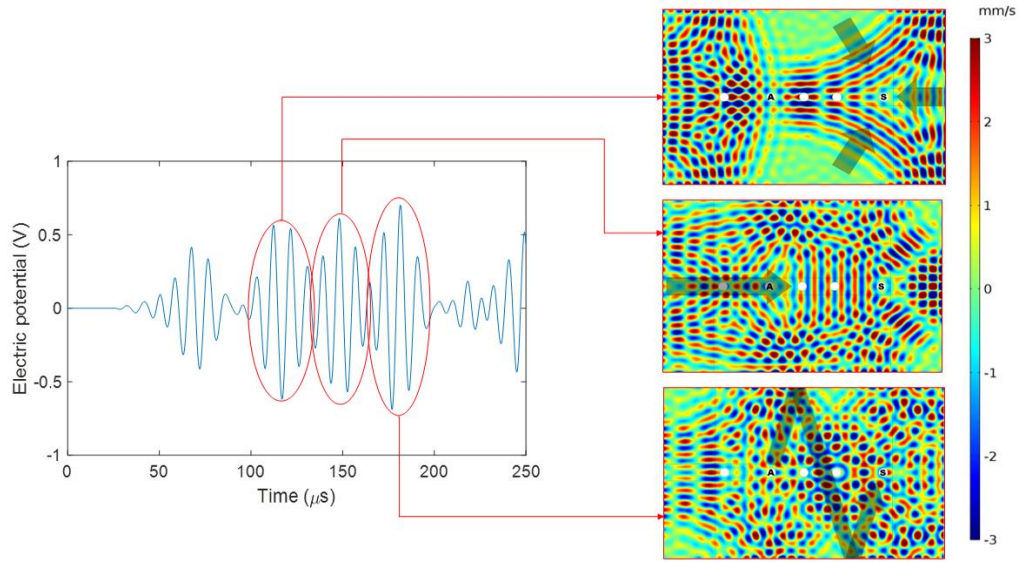


Figure 23. Sensed signal in Plate 1 divided into packets where every packet is specified based on the obtained wave field.

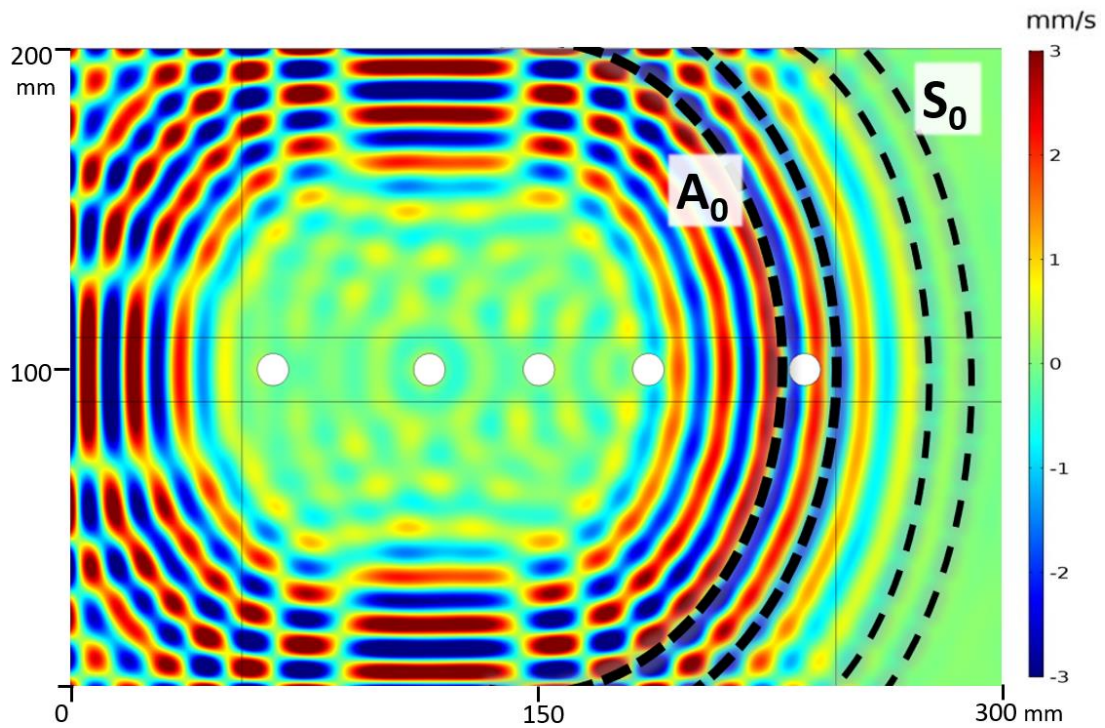


Figure 24. Out-of-plane velocity wavefield showing excited S₀ and A₀ modes

The second difference is shown in the fourth packet or P4. This time plates 1 and 3 have the same low amplitude compared to plate 2. The first part of this packet is from

the second reflections of A_0 from the top and bottom sides, this is the same for all plates. However, the second part of this packet is only noticed in plate 2 due to the two bent edges and the reflected and transmitted waves from both edges. Figure 28 shows the four reflections that hit the sensor at this time interval which are only detected in plate 2 at this specific time. Plate 1 does not have the bent edges at all and plate 3 has a longer distance at its right side bent edge which also does not allow these reflections to hit the sensor at the time given. This analysis from COMSOL allowed the bent edges and their effect on transmission and reflections to be shown and studied more profoundly than only theoretically.

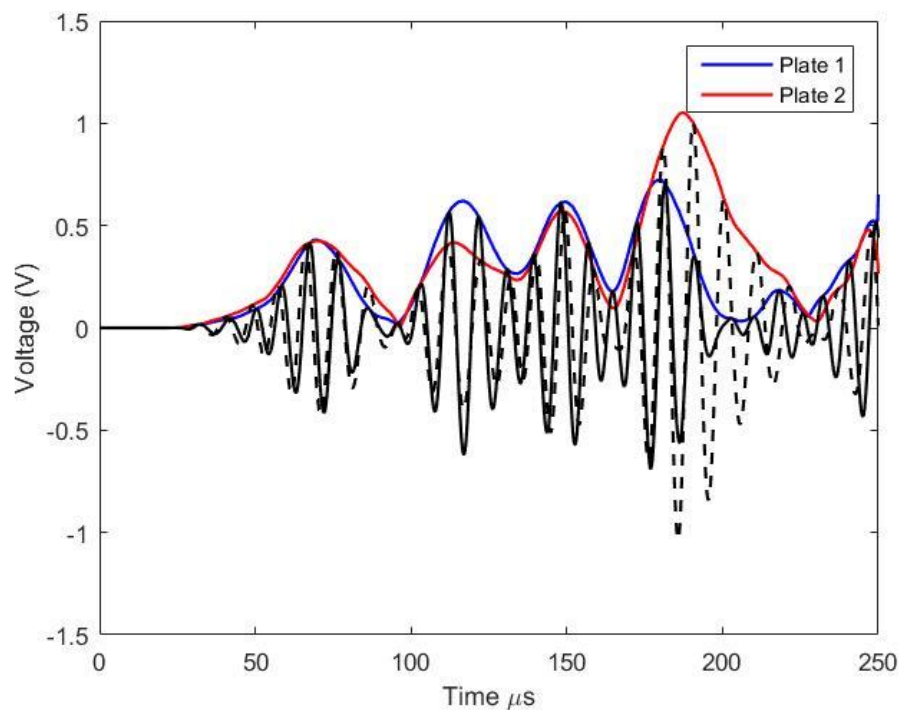


Figure 25. Measured signal and envelope tracing

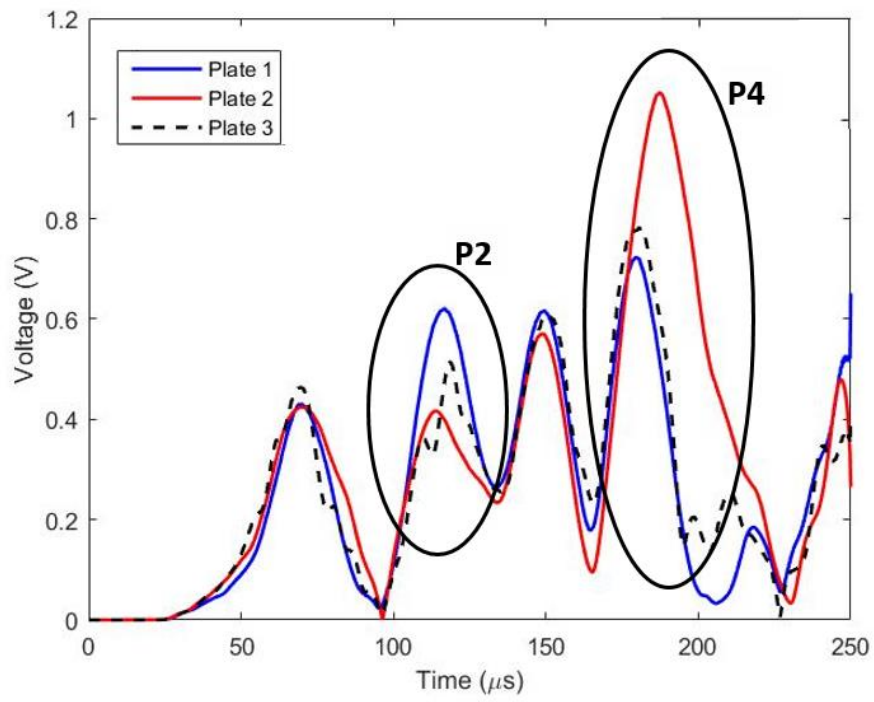


Figure 26. Measured signal envelopes for each plate

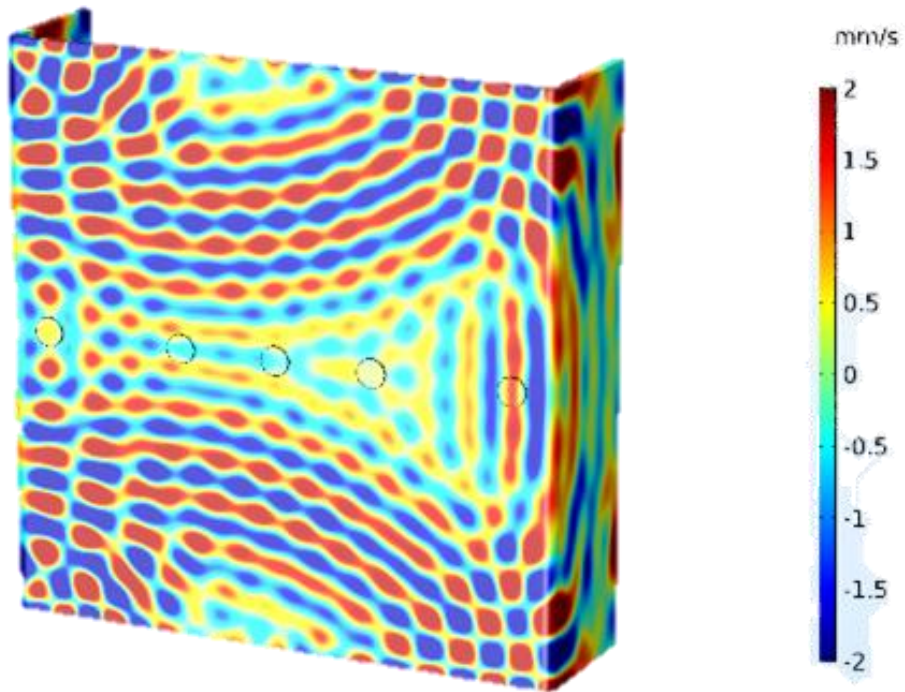


Figure 27. Reflection and transmission wave field from the right side bent-edge in Plate 2

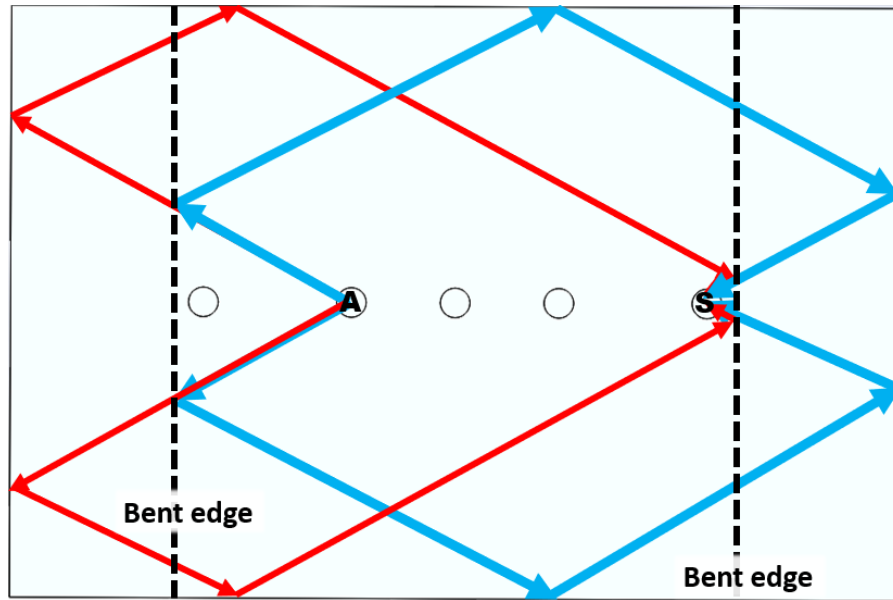


Figure 28. Four pathway reflections in plate 2

B. The Study of Boundary Reflection and Attenuation of Lamb Waves in an Aluminum Plate

1. The built-up signal according to the theorem

The distances of the first, second, and third reflections for every plate is determined using the boundary reflection theory mentioned. With the assistance of the waveform revealer, a normalized signal containing the chosen modes can be obtained for each calculated distance. However, the assumed overall signal at this point does not take into account the wave attenuation in the plate or the reflection coefficients. The attenuations for the propagating wave at both frequencies were obtained experimentally by scanning a horizontal line on plate L in-line with the actuating PZT with a 50 mm increments using the LDV. The normalized amplitudes of the obtained signals were plotted against the traveled distance in Figure 29. A curve fit is drawn using MATLAB software for the normalized data and the curve equations were then obtained:

$$At_{@ 100 \text{ kHz}} = 2.145x^{-0.47} \quad (8)$$

$$At_{@ 200 \text{ kHz}} = 2.273x^{-0.5095}$$

where At is the attenuation value and x is the distance covered by the wave. From that on, all obtained signals for all required distances were multiplied by the attenuation value.

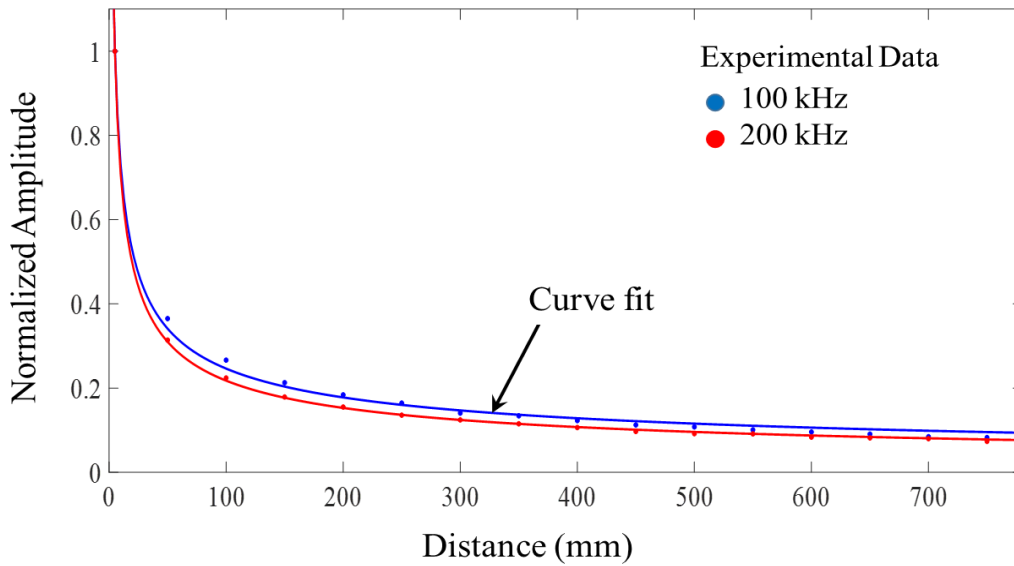


Figure 29. A0 Lamb wave mode attenuation curve was generated experimentally.

The reflection coefficient was also predicted by finding the ratio of the amplitude of the reflected signal to that of the incident signal for the specified mode. It was, however, important to keep the same propagation distance when comparing the reflected and the incident signal. The direct incident propagating distance used for this analysis is DL_0 as shown in Figure 30. The reflected signals were analyzed at different angles varying between 0° and 60° with 5° increments such that the traveled reflection distance from the actuator to the sensing point maintained the same value as DL_0 . All

obtained coefficients ranged between 0.96 and 0.99 and thus we considered the average of 0.98 to be used for all propagating angles.

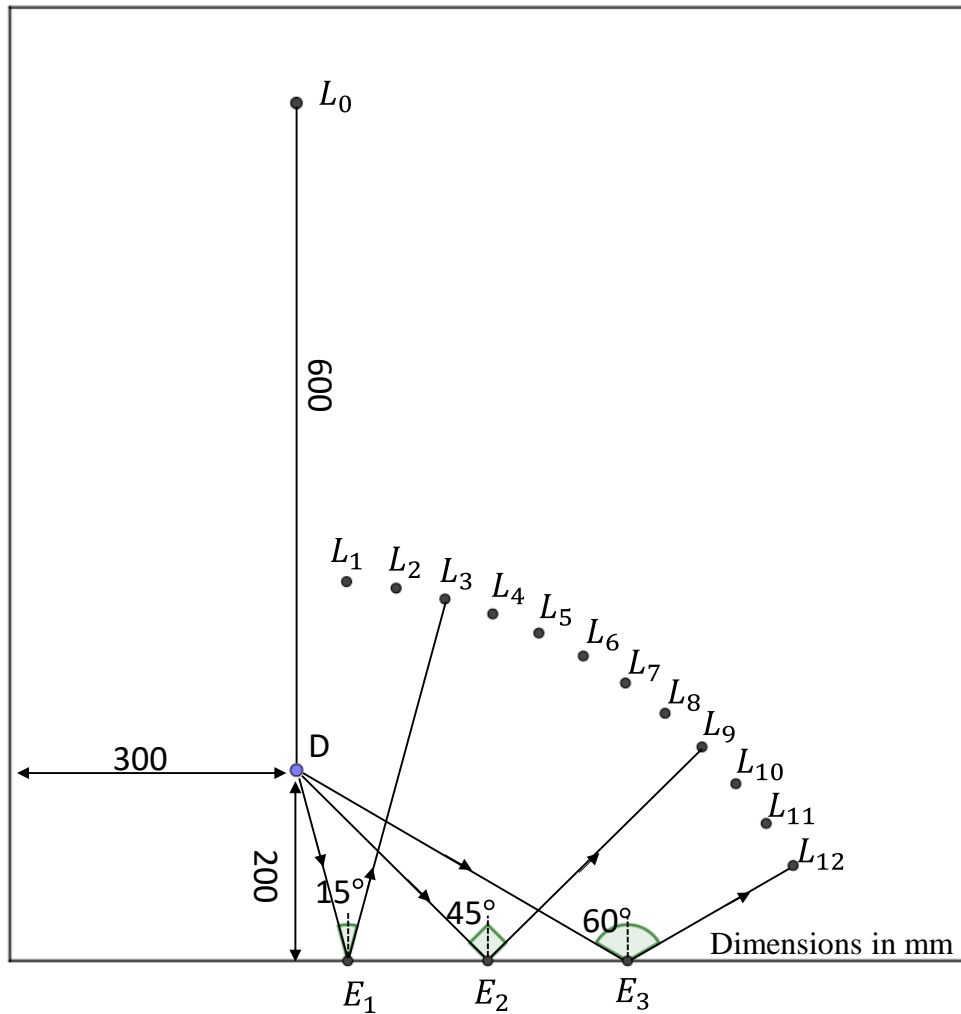


Figure 30. Experimental setup schematic for calculating Lamb wave boundary reflection (LBR) coefficient.

After obtaining the attenuation and reflection coefficients, the predicted overall signal of a propagating Lamb wave could be then obtained. In the first analysis, only the top boundary reflection is added to the incident signal and then compared to the experimental results from region 2 in plate L. The obtained signals were plotted against the LDV results in Figure 31a and 29b, respectively. Secondly, the left, bottom and corner boundary reflections were added to the first received signal and then compared to

the experimental results from region 3 in plate L as shown in Figure 31c and 29d.

Similar results were also obtained for the plate S using the LBR theorem. All predicted signals at the 100 and 200 kHz frequencies gave an excellent match with the experiment results for the A_0 mode.

However, since the one-dimensional laser vibrometer measures the out-of-plane velocity, the S_0 mode was hardly detected in our LDV data.

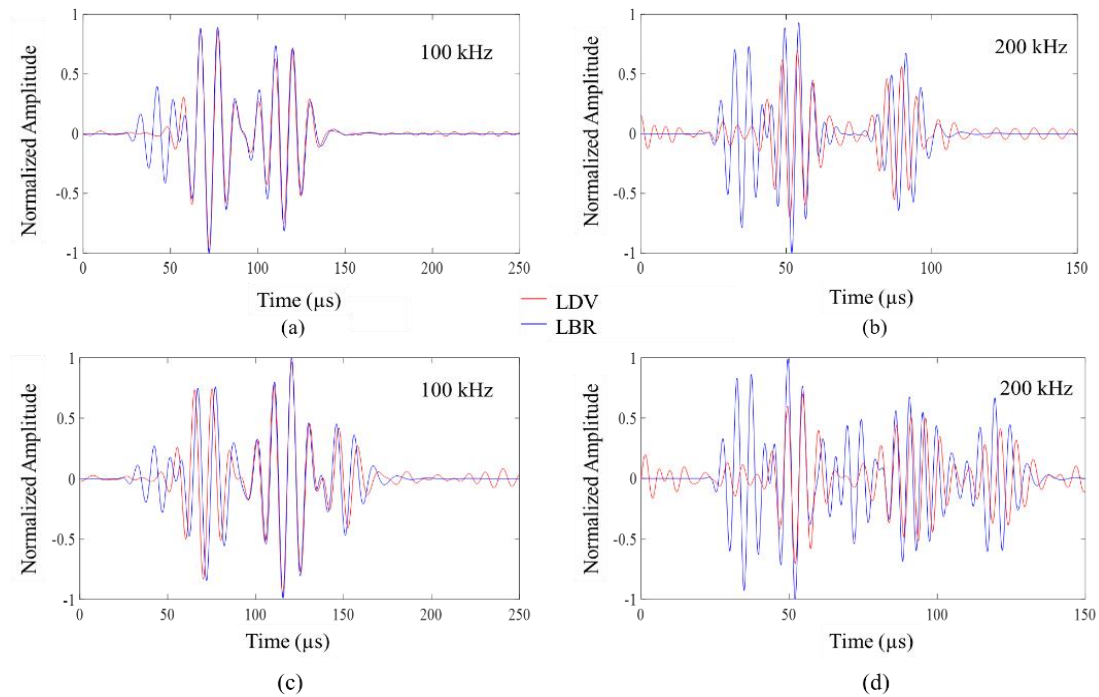


Figure 31. Lamb wave boundary reflection (LBR) theorem versus experimental results at 100 and 200 kHz excitation frequencies in region 2 of plate L (a,b) and region 3 of plate L (c,d).

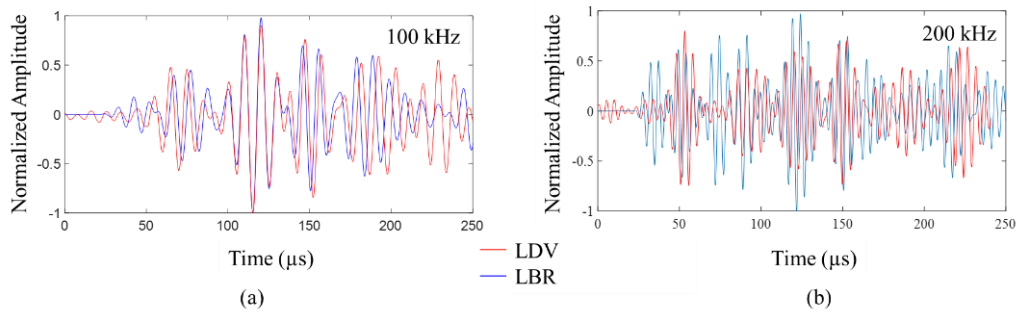


Figure 32. Lamb wave boundary reflection (LBR) theorem versus experimental results at 100 and 200 kHz excitation frequencies in plate S.

C. Effect of the angle of the bent on lamb wave in an aluminum plate

PZT A was used as an actuator and two sets of results were taken, results from PZT B, and results taken by the LDV over a line scan Line 1 and Line 2 located 20 mm before and after the bent respectively. Based on the results obtained from the line scan for

1. Effect of bent on the wave propagation

Comparing the results after each bent with the reference one (no bent) at 100 kHz for line scan 1 in figure 33 shows the following.

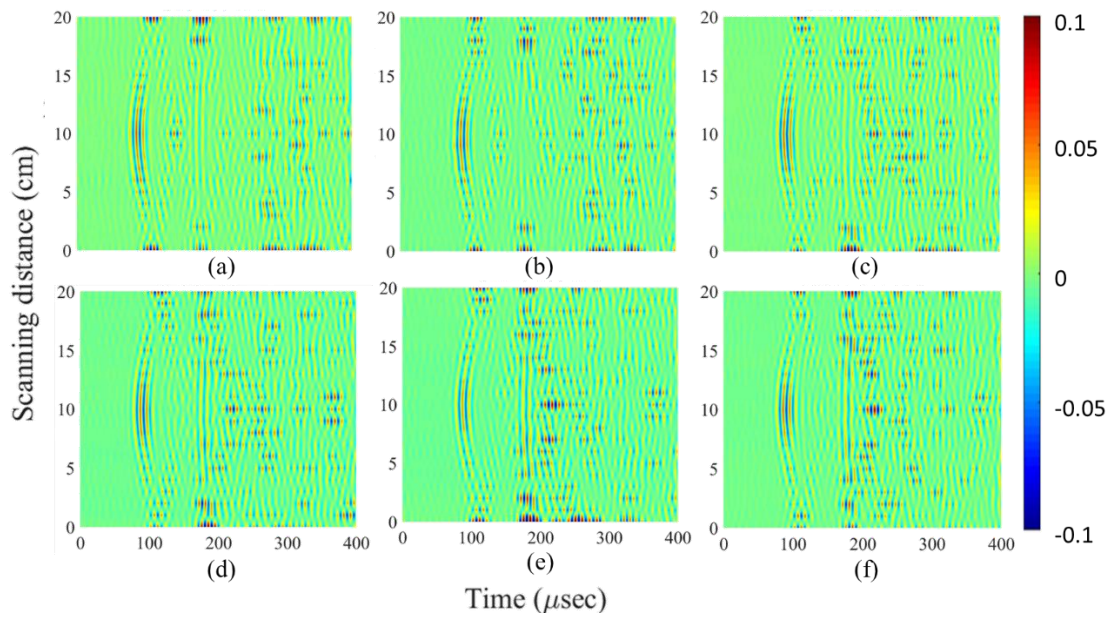


Figure 33 The line scan 1 for the plate at 100 kHz (a) 0 degree (b) 30 degree (c) 60 degree (d) 90 degree (e) 120 degree and (f) 150 degree

First, the direct signal which is the first packet is the same for all and this is because nothing changes between the actuator and the sensing points. However, this packet has widened a bit moving from 0 to angle 150 degree and this is due to the first reflection from the bent which it seems to be a constructive wave that adds to the first received signal. Second, the second packet at time 130 μ s is the reflection from the top and bottom. It remained to appear regardless of the bent however it decreases in amplitude. Third, the third packet which is the first reflection from the right edge at time 166 μ s was clear at the reference plate but after the bent is done this reflection decreases as we increase the bent from 0 to 120 until it vanished at the 150 degree bend. Fourth, at 178 μ s there was a packet that its energy increased with each bent and this is due to the second reflection from the bent shown in figure 34

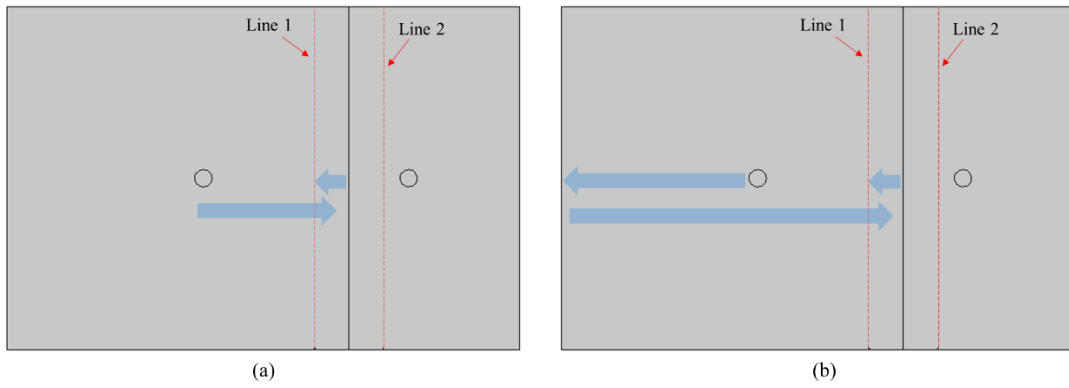


Figure 34 Top view of the plate showing the reflection from the bent (a) the first reflection and (b) the second reflection

After doing the comparison on the first line scan, Line 1, a Comparison was made on the second line of the scan, line 2, which is located after the bent. Figure 35 shows the results of the line scan after each bent and the results go as follows.

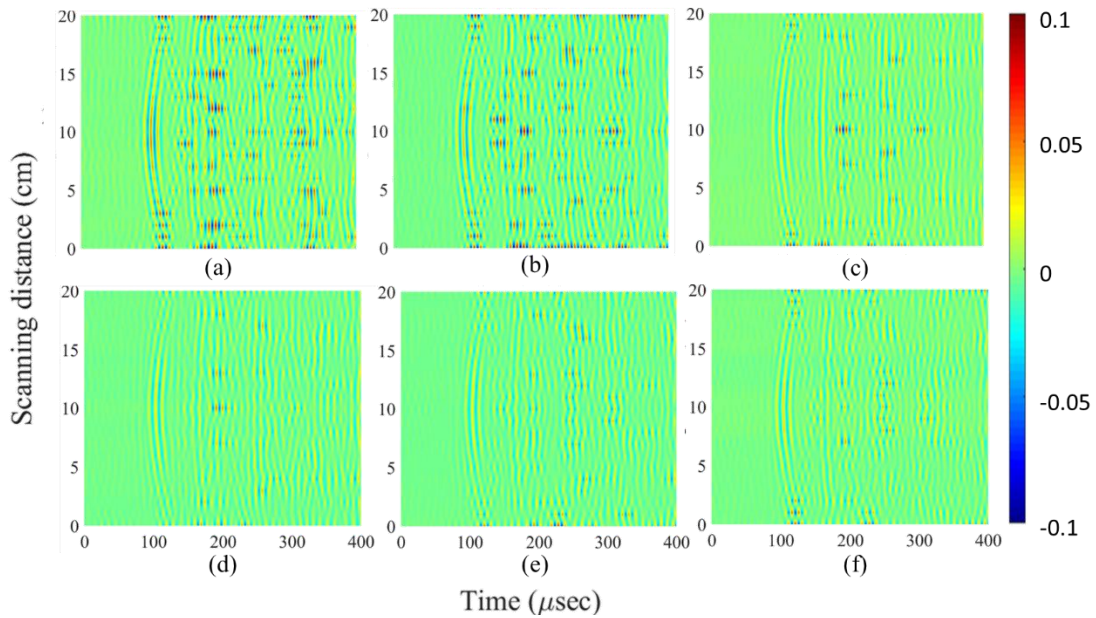


Figure 35 The line scan 2 for the plate at 100 kHz (a) 0 degree (b) 30 degree (c) 60 degree (d) 90 degree (e) 120 degree and (f) 150 degree

First, the first packet has decreased in amplitude between 0 *degree* and 90 *degree*, this is due to the effect of the bent where it reflects part of the wave and allows the other part to pass which affect the amplitude. Second, at 136 μ s there was the top and bottom reflection shown in the figure that appears on the plate before being bent. These reflections decreased after bending 30 *degree* and disappeared after increasing the bent angle above 60 *degree*, this is because the bent makes a barrier between the reflection and the sensing point leading to a decrease in amplitude and it couldn't be well detected by the sensing point.

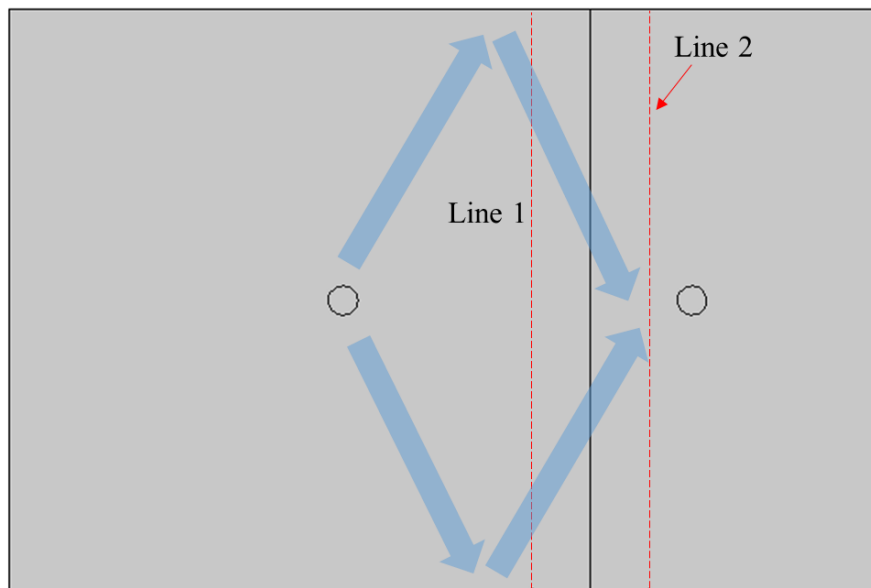


Figure 36 Top and bottom reflection for the second line of scan showing how the bent blocks the way of the wave

A similar analysis was done for the frequency of 200 *kHz* which shows the effect of the bent on the signal. Here the comparison is going to be between the two lines of scan Line 1 which is located 20 mm before the bent and line 2 which is located 20 mm after the bent as shown in figure 9.

Results shown in figure 38 for line scan 2 which is after the bent shows a decrease in energy as the bent angle increases compared to 0 *degree* bent. Figure 38 shows minimal values since part of the signal passes the bent and was trapped in the small side where the reflection increases and makes the signal. However, figure 37 shows clear signals and complete reflected signals for a time below 200 μ s since in this part more percentage of the wave exists and the area of this side is larger than that of the left side.

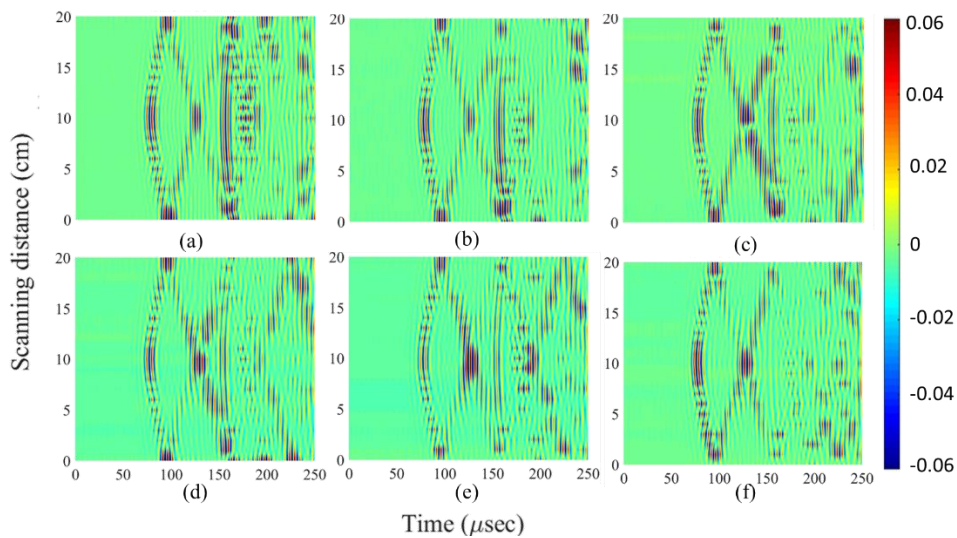


Figure 37. The line scan 1 for the plate at 200 kHz (a) 0 *degree* (b) 30 *degree* (c) 60 *degree* (d) 90 *degree* (e) 120 *degree* and (f) 150 *degree*

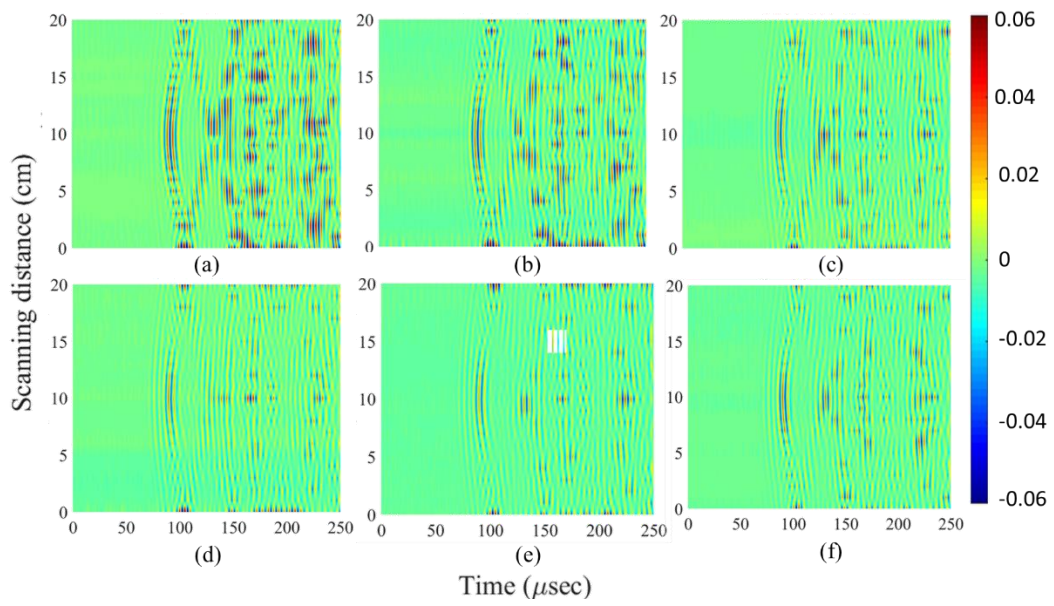


Figure 38. The line scan 2 for the plate at 200 kHz (a) 0 degree (b) 30 degree (c) 60 degree (d) 90 degree (e) 120 degree and (f) 150 degree

CHAPTER VII

CONCLUSION AND FUTURE WORK

Lamb waves are elastic guided waves known for their long-distance propagation in thin structures, so they are used to study the health of a material. However, the multimode propagation, the mode conversion, and the boundary reflections make the interpretation process challenging.

This study focused on the interpretation of the boundary reflection of Lamb Waves. Both experimental and computational analyses were done and the obtained results were analyzed and compared with each other. The study started by understanding the wave propagation in the plate where the results obtained analytically from both COMSOL and ABAQUS gave a visualization for the wave in the plate and how it interacts with the boundaries and the bent. After that, another experiment was made on an infinitely large plate, and PZTs were located in a way that eliminates the boundary reflection each time. This reflection with the aid of the visualized wave scattering helped in creating the BRF which found the location of virtual actuators that can help find the distance traveled by the wave after it is reflected from the edges. With the aid of the WaveForm Revealer, an assumed signal was predicted that matches to an excellent extent the signal obtained experimentally after adding the attenuation and the reflection coefficient. To move towards more complex structures a new experiment was also done that studied the effect of a bent on the signal, for that different angles were taken and the results were analyzed.

This study gave a clear vision of Lamb Wave boundary reflections and will form a starting point to predict the wave propagation and effect of bends in a structure. It will simplify the analysis process of those waves by predicting the boundary reflections and

eliminating them from the signal. This will form a clean signal without boundary reflection which helps in focusing other reflections such as cracks or other material deformation.

More studies can be done on this topic. First, finding a relation between the bent angle and what percentage of the wave is reflected after hitting the bent. Second, do these results still applicable for non-homogeneous materials? Finally, is it possible to predict all boundary reflection in a complex structure material? All these questions need more work and studies that might make a step forward in the SHM domain and facilitate the analysis process.

REFERENCES

1. Cartz, L., *Nondestructive Testing*. 1995.
2. Giurgiutiu, V., *Structural health monitoring: with piezoelectric wafer active sensors*. 2007: Elsevier.
3. Karbhari, V.M., *Non-destructive evaluation (NDE) of polymer matrix composites*. 2013: Elsevier.
4. Zhao, M., et al., *Mode identification and extraction of broadband ultrasonic guided waves*. *Measurement Science and Technology*, 2014. **25**(11).
5. Kim, B. and Y. Roh, *Simple expressions of the reflection and transmission coefficients of fundamental Lamb waves by a rectangular notch*. *Ultrasonics*, 2011. **51**(6): p. 734-44.
6. Travaglini, C., et al., *Feasibility of high frequency guided wave crack monitoring*. *Structural Health Monitoring*, 2017. **16**(4): p. 418-427.
7. Kim, H.-W. and F.-G. Yuan, *Enhanced damage imaging of a metallic plate using matching pursuit algorithm with multiple wavepaths*. *Ultrasonics*, 2018. **89**: p. 84-101.
8. Sridharan, S., *Delamination behaviour of composites*. 2008: Elsevier.
9. Philibert, M., et al., *Damage detection in a composite T-joint using guided lamb waves*. *Aerospace*, 2018. **5**(2): p. 40.
10. Pieczonka, Ł., et al., *Damage detection in composite panels based on mode-converted Lamb waves sensed using 3D laser scanning vibrometer*. *Optics and lasers in engineering*, 2017. **99**: p. 80-87.
11. Joseph, L.R., *Ultrasonic Guided Waves in Solid Media*. 2014.
12. Schmerr, L.W., *Fundamentals of ultrasonic nondestructive evaluation*. 2016: Springer.
13. Harb, M. and F. Yuan, *A rapid, fully non-contact, hybrid system for generating Lamb wave dispersion curves*. *Ultrasonics*, 2015. **61**: p. 62-70.
14. Harb, M.S. and F.-G. Yuan, *Air-Coupled Nondestructive Evaluation Dissected*. *Journal of Nondestructive Evaluation*, 2018. **37**(3): p. 50.
15. Lu, Y., et al., *Quantitative evaluation of crack orientation in aluminium plates based on Lamb waves*. *Smart Materials and Structures*, 2007. **16**(5): p. 1907.
16. Lu, Y., L. Ye, and Z. Su, *Crack identification in aluminium plates using Lamb wave signals of a PZT sensor network*. *Smart Materials and Structures*, 2006. **15**(3): p. 839.
17. Li, F., H. Peng, and G. Meng, *Quantitative damage image construction in plate structures using a circular PZT array and lamb waves*. *Sensors and Actuators A: Physical*, 2014. **214**: p. 66-73.
18. Santhanam, S. and R. Demirli, *Reflection of Lamb waves obliquely incident on the free edge of a plate*. *Ultrasonics*, 2013. **53**(1): p. 271-82.
19. Nazeer, N., M. Ratssepp, and Z. Fan, *Damage detection in bent plates using shear horizontal guided waves*. *Ultrasonics*, 2017. **75**: p. 155-163.
20. *COMSOL Multiphysics* COMSOL, Inc: Stockholm, Sweden.
21. Ciang, C.C., J.-R. Lee, and H.-J. Bang, *Structural health monitoring for a wind turbine system: a review of damage detection methods*. *Measurement science and technology*, 2008. **19**(12): p. 122001.

22. Antoniadou, I., et al., *Aspects of structural health and condition monitoring of offshore wind turbines*. Philosophical Transactions of the Royal Society A: Mathematical, Physical and Engineering Sciences, 2015. **373**(2035): p. 20140075.
23. Staszewski, W., C. Boller, and G.R. Tomlinson, *Health monitoring of aerospace structures: smart sensor technologies and signal processing*. 2004: John Wiley & Sons.
24. Okasha, N.M., et al., *Reliability analysis and damage detection in high-speed naval craft based on structural health monitoring data*. Structural Health Monitoring, 2011. **10**(4): p. 361-379.
25. Soliman, M., G. Barone, and D.M. Frangopol, *Fatigue reliability and service life prediction of aluminum naval ship details based on monitoring data*. Structural Health Monitoring, 2015. **14**(1): p. 3-19.
26. Chang, P.C., A. Flatau, and S. Liu, *Health monitoring of civil infrastructure*. Structural health monitoring, 2003. **2**(3): p. 257-267.
27. Karbhari, V.M. and F. Ansari, *Structural health monitoring of civil infrastructure systems*. 2009: Elsevier.
28. Deraemaeker, A. and K. Worden, *New trends in vibration based structural health monitoring*. Vol. 520. 2012: Springer Science & Business Media.
29. Giurgiutiu, V., *Tuned Lamb wave excitation and detection with piezoelectric wafer active sensors for structural health monitoring*. Journal of intelligent material systems and structures, 2005. **16**(4): p. 291-305.
30. Gopalakrishnan, S., M. Ruzzene, and S. Hanagud, *Computational techniques for structural health monitoring*. 2011: Springer Science & Business Media.
31. Eivani, A.R., et al., *Microstructural evolution and fatigue properties of severely deformed AA1050 aluminum alloy*. Materials Characterization, 2017. **130**: p. 204-210.
32. Roh, H.D., et al., *Deformation and interlaminar crack propagation sensing in carbon fiber composites using electrical resistance measurement*. Composite Structures, 2019. **216**: p. 142-150.
33. Royer, D. and E. Dieulesaint, *Elastic waves in solids I: Free and guided propagation*. 1999: Springer Science & Business Media.
34. Viktorov, I., *Rayleigh and Lamb waves: physical theory and applications*. Chapter II, 1967.
35. Memmolo, V., et al., *Guided wave propagation and scattering for structural health monitoring of stiffened composites*. Composite structures, 2018. **184**: p. 568-580.
36. Mitra, M. and S. Gopalakrishnan, *Guided wave based structural health monitoring: A review*. Smart Materials and Structures, 2016. **25**(5): p. 053001.
37. Xu, C.-b., et al., *A guided wave dispersion compensation method based on compressed sensing*. Mechanical Systems and Signal Processing, 2018. **103**: p. 89-104.
38. Xu, K., et al., *Mode separation of Lamb waves based on dispersion compensation method*. The Journal of the Acoustical Society of America, 2012. **131**(4): p. 2714-2722.
39. Moll, J., et al., *Open Guided Waves: online platform for ultrasonic guided wave measurements*. Structural Health Monitoring, 2019. **18**(5-6): p. 1903-1914.

40. Chandarana, N., et al., *Early damage detection in composites during fabrication and mechanical testing*. *Materials*, 2017. **10**(7): p. 685.
41. Chen, X., et al., *Composite damage detection based on redundant second-generation wavelet transform and fractal dimension tomography algorithm of lamb wave*. *IEEE transactions on instrumentation and measurement*, 2012. **62**(5): p. 1354-1363.
42. Alleyne, D. and P. Cawley, *A two-dimensional Fourier transform method for the measurement of propagating multimode signals*. *The Journal of the Acoustical Society of America*, 1991. **89**(3): p. 1159-1168.
43. Michaels, T.E., J.E. Michaels, and M. Ruzzene, *Frequency–wavenumber domain analysis of guided wavefields*. *Ultrasonics*, 2011. **51**(4): p. 452-466.
44. Ruzzene, M., *Frequency-wavenumber domain filtering for improved damage visualization*, in *Ultrasonic And Advanced Methods For Nondestructive Testing And Material Characterization*. 2007, World Scientific. p. 591-611.
45. Horace, L., *On Waves in an Elastic Plate*. Royal Society, 1916.
46. Su, Z., L. Ye, and Y. Lu, *Guided Lamb waves for identification of damage in composite structures: A review*. *Journal of sound and vibration*, 2006. **295**(3-5): p. 753-780.
47. Green Jr, R.E., *Non-contact ultrasonic techniques*. *Ultrasonics*, 2004. **42**(1-9): p. 9-16.
48. Harb, M.S. and F.-G. Yuan, *Damage imaging using non-contact air-coupled transducer/laser Doppler vibrometer system*. *Structural Health Monitoring*, 2016. **15**(2): p. 193-203.
49. (LAMSS), L.f.A.M.a.S.S., *Wavescope 2010*: University of South Carolina
50. (LAMSS), L.f.A.M.a.S.S., *Waveform Revealer*. 2012: University of South Carolina.
51. Ghose, B., et al., *Two Dimensional FEM Simulation of Ultrasonic Wave Propagation in Isotropic Solid Media using COMSOL*, in *COMSOL Conference 2010 India*.

